

RNAi as a Potential Targeted Therapy in Oculopharyngeal Muscular Dystrophy

Kavin Tamizhmani

Division of Clinical and Translational Research, McGill University, Montreal

September 2024

A thesis submitted to McGill University in partial fulfillment of the requirements of
the degree of Master of Science

© Kavin Tamizhmani, 2024

TABLE OF CONTENTS

ABSTRACT	4
RÉSUMÉ	5
ACKNOWLEDGEMENTS	7
CONTRIBUTION OF AUTHORS	8
LIST OF FIGURES	9
LIST OF TABLES	10
LIST OF ABBREVIATIONS	11
CHAPTER 1: INTRODUCTION	15
1.1 Trinucleotide Repeat Disorders	15
CHAPTER 2: LITERATURE REVIEW	17
2.1 Mechanism of Repeat Formation	17
2.2 Oculopharyngeal Muscular Dystrophy (OPMD).....	18
2.3 OPMD treatment options.....	19
2.4 RNAi	22
2.5 RNAi Therapy in Monogenic and Trinucleotide Repeat Neurological Diseases	24
2.6 RNAi Therapy in OPMD	25
2.7 Rationale and Objectives	25
CHAPTER 3: MATERIALS AND METHODS	27
3.1 MiRNA Plasmid	27
3.3 PABPN1 Ala-10/17 Dsred Plasmids	30
3.4 MiRNA transfection into HEK293T and C2C12 cells.....	31
3.5 Fluorescence microscopy.....	33
3.6 Protein Extraction	33

3.7 RNA Extraction	34
3.8 Western Blot.....	35
3.9 Quantitative RT-PCR.....	37
CHAPTER 4: RESULTS	39
4.1 Fluorescent Imaging of HEK293T and C2C12 transfected cells	39
4.2 Western blot of miRNA 2-induced PABPN1 knockdown in HEK293T	40
4.3 RT-qPCR of miRNA 2-induced PABPN1 knockdown in HEK293T	44
CHAPTER 5: DISCUSSION	46
5.1 miRNA effectively silences PABPN1 Ala-10/17 at the protein and RNA levels	46
5.2 Study limitations	47
5.3 Future directions.....	49
CHAPTER 6: CONCLUSION.....	53
REFERENCES.....	55

Abstract

Oculopharyngeal muscular dystrophy (OPMD) is a late adult-onset autosomal disease characterized by progressive dysphagia, eyelid ptosis and proximal limb weakness. Previous studies have identified the polyadenylate-binding protein nuclear 1 (*PABPN1*) as the cause of disease etiology. Wildtype *PABPN1* Ala-10 contains a GCN repeat encoding polyalanine at the 5' end, whereas the mutated form of the gene has a GCG repeat expansion varying from 11-18 consecutive trinucleotide repeats. Currently, no curative medical treatment is available for OPMD.

MicroRNA (miRNA) therapy presents as a potential treatment strategy based on its employment in the successful treatment of other neurological trinucleotide repeat diseases. In this study, the primary aims were to design miRNA constructs and evaluate their capacity to effectively and selectively target the expanded *PABPN1* Ala-17 repeat in a discriminatory manner, sparing the wildtype *PABPN1* Ala-10 allele which must be ubiquitously expressed as it is essential for cell survival. Therefore, 12 miRNA constructs were synthesized to preferentially target the *PABPN1* expanded repeat allele at various regions of the transcript. Of the 12 constructs, 1 of the candidates, miRNA 2, was initially selected for evaluation in HEK293T and C2C12 OPMD cell lines based on its design targeting the *PABPN1* gene spanning the 5' region of the gene and certain promoter elements to the left flanking adjacent upstream region.

Preliminary western blot and RT-qPCR findings confirmed the effectiveness of miRNA 2 as a targeted therapy but did not show the ability of miRNA 2 to selectively knockdown *PABPN1* Ala-17 with a higher relative affinity. Overall, the confirmation of miRNA as an effective targeted therapy in OPMD is encouraging and warrants further testing of the other synthesized miRNA constructs to achieve the ultimate goal of selective cleavage.

Résumé

La dystrophie musculaire oculopharyngée (OPMD) est une maladie autosomique à apparition tardive de l'adulte caractérisée par une dysphagie progressive, un ptosis des paupières et une faiblesse des membres proximaux. Des études antérieures ont identifié la protéine nucléaire 1 de liaison au polyadénylate (*PABPN1*) comme la cause de l'étiologie de la maladie. Le type sauvage *PABPN1* Ala-10 contient une répétition GCN codant pour la polyalanine à l'extrémité 5', alors que la forme mutée du gène a une expansion de répétition GCG variant de 11 à 18 répétitions trinuécléotidiques consécutives. Actuellement, aucun traitement médical curatif n'est disponible pour l'OPMD.

La thérapie par microARN (miARN) se présente comme une stratégie de traitement potentielle basée sur son utilisation dans le traitement réussi d'autres maladies neurologiques à répétition trinuécléotidique. Dans cette étude, les principaux objectifs étaient de concevoir des constructions de miARN et d'évaluer leur capacité à cibler efficacement et sélectivement la répétition élargie de *PABPN1* Ala-17 de manière discriminatoire, en épargnant l'allèle sauvage *PABPN1* Ala-10 qui doit être exprimé de manière omniprésente car il est essentiel pour la survie des cellules. Par conséquent, 12 constructions de miARN ont été synthétisées pour cibler préférentiellement l'allèle répété étendu *PABPN1* dans diverses régions du transcrit. Parmi les 12 constructions, l'un des candidats, le miARN 2, a été initialement sélectionné pour évaluation dans les lignées cellulaires HEK293T et C2C12 OPMD sur la base de sa conception ciblant le gène *PABPN1* couvrant la région 5' du gène et certains éléments promoteurs du flanc gauche adjacent région amont.

Les résultats préliminaires du Western blot et de la RT-qPCR ont confirmé l'efficacité du miARN 2 en tant que thérapie ciblée, mais n'ont pas montré la capacité du miARN 2 à inhiber

sélectivement PABPN1 Ala-17 avec une affinité relative plus élevée. Dans l'ensemble, la confirmation du miARN en tant que thérapie ciblée efficace dans l'OPMD est encourageante et justifie des tests plus approfondis sur les autres constructions de miARN synthétisées afin d'atteindre l'objectif ultime du clivage sélectif.

Acknowledgements

I would like to express my sincere gratitude to my supervisors, Dr. Guy Rouleau and Dr. Patrick Dion, for their supervision, guidance and patience throughout my studies. Additionally, I would like to extend my sincere appreciation to my mentor Dr. Aida Abu-Baker for supervising my project, training and assisting me with all laboratory experiments. I am grateful for the valuable feedback and suggestions provided by the members of my supervisory committee: Dr. Miltiadis Paliouras, Dr. Bernard Brais and Dr. Nicholas Dumont. I would also like to thank all members of the Rouleau laboratory for their timely assistance, especially Dr. Helene Catoire and Daniel Rochefort for their assistance with cell lines and laboratory techniques. Finally, I would like to thank my family for their constant support throughout this endeavor.

Contribution of Authors

The thesis manuscript was written entirely by Kavin Tamizhmani under the supervision of Dr. Guy Rouleau, Dr. Patrick Dion and Dr. Aida Abu-Baker. Experimental design, data collection and analysis of findings were completed by Kavin Tamizhmani with guidance from Dr. Guy Rouleau, Dr. Patrick Dion and Dr. Aida Abu-Baker.

List of Figures

Figure 1: RNAi pathways of siRNA and miRNA

Figure 2: Invitrogen BLOCK-iT Pol II miR RNAi pcDNA GFP expression vector

Figure 3: 5' to 3' Bsa1 forward and reverse single stranded linker oligos

Figure 4: Bsa1 restriction enzyme recognition site, restriction digest product and overhang

Figure 5: *PABPN1* ATG start codon (red), GCG repeat tract (yellow) and miRNA target region (underline)

Figure 6: 1% agarose DNA gel: Lane 1 (L1)-1 kb plus ladder, L2- miRNA1, L3- miRNA2, L4- negative control

Figure 7: HEK293T 12-well plate transfection layout with 1 µg of plasmid DNA (Jet prime)

Figure 8: miRNA2, PABPN1 Ala-10/17 and miRNA 7-2 in HEK293T cells 48-72 hours post transfection

Figure 9: miRNA2, PABPN1 Ala-10/17 and miRNA 7-2 in C2C12 cells 48-72 hours post transfection

Figure 10: Western blot of miRNA 2-induced PABPN1 knockdown in HEK293T cells

Figure 11: Relative PABPN1 Ala-10 expression after miRNA 2-induced knockdown

Figure 12: Relative PABPN1 Ala-17 expression after miRNA 2-induced knockdown

Figure 13: RT-qPCR of relative PABPN1 expression after miRNA 2-induced knockdown

Figure 14: Relative endogenous PABPN1 expression in the presence of PABPN1 Ala-10/17

List of Tables

Table 1: HEK293T miRNA 2-induced PABPN1 Ala-10/17 knockdown western blot densitometry calculations

Table 2: Endogenous PABPN1 western blot densitometry calculations in the presence of PABPN1 Ala-10/17

List of Abbreviations

OPMD	Oculopharyngeal muscular dystrophy
PABPN1	Polyadenylate-binding protein nuclear 1
GCN/(GCA) _n	Variable polyalanine repeat sequence
GCG	Nucleic acid sequence encoding the amino acid alanine
RNAI	RNA interference
MIRNA	Micro RNA
TRD	Triplet repeat diseases
STR	Short tandem repeats
LOF	Loss-of-function
GOF	Gain-of-function
FRAXA/FRAXE	Fragile X disorder genes
UTR	Untranslated region
<i>FMRI</i>	Fragile X mental retardation 1 gene
HD	Huntington's disease
SCA1	Spinocerebellar Ataxia Type 1
POLYQ	Polyglutamine
ALA	Alanine
MRI	Magnetic resonance imaging
INI	Intranuclear inclusions
NLS	Nuclear localization signal
GFP	Green Fluorescent Protein
CP	Cricopharyngeal

HSP40/HSP70	Heat shock protein 40/70
VHH	Single-domain antibody reagents
SIRNA	Small interfering RNA
PRI-MIRNA	Primary precursor miRNA
DROSHA	Nuclear RNase III
EXP5	Exportin 5
DICER	Endoribonuclease RNase III
AGO	Argonaut
RISC	RNA-Induced Silencing Complex
MIRISC	Micro RNA RNA-Induced Silencing Complex
DMD	Duchenne's Muscular Dystrophy
SMA	Spinal Muscle Atrophy
MJD	Machado-Joseph Disease
<i>ATXN3</i>	Ataxin-3
<i>HTT</i>	Huntingtin
AAV	Adeno-associated virus
HHRZS	Hammerhead ribozymes
OPTPABPN1	Optimized PABPN1
HEK293T	Human Embryonic Kidney cells
C2C12	Murine myoblast cells
RT-QPCR	Reverse transcription-quantitative polymerase chain reaction
CMV	Cytomegalovirus
Bsa1	Restriction enzyme/cut site

CDNA	Complementary DNA
NTS	Nucleotides
P	Passenger
G	Guide
MIRNA 2	Micro RNA 2
DSRED/RFP	Red Fluorescent Protein
ALA-10	Alanine-10
ALA-17	Alanine-17
DPBS	Dulbecco's Phosphate Buffered Saline
SUB	Sodium sulfate utilizing buffer
BSA	Bovine serum albumin
DEPC	Diethyl pyrocarbonate
RNAP	RNA polymerase II
NT	Non-transfected
CT	Cycle threshold
$\Delta\Delta CT$	Comparative cycle threshold
MIRNA 7-2	Micro RNA 7-2 positive control
KDA	Kilodalton
RT	Reverse transcription
RQ	Reverse quantification
ALS	Amyotrophic lateral sclerosis
AD	Alzheimer's disease
TDP-43	TAR DNA-binding protein 43

FTD	Frontotemporal dementia
MSUT2	Mammalian suppressor of tauopathy 2
CRC	Colorectal cancer
CCA	Cervical cancer
CCRCC	Clear renal cell carcinoma
BC	Bladder cancer

Chapter 1: Introduction

1.1 Trinucleotide Repeat Disorders

Trinucleotide repeat disorders, also known as triplet repeat diseases (TRD), consist of over 40 neurodegenerative disorders [1]. The repetitive elements of the human genome responsible for TRD are referred to as short tandem repeats (STR) or microsatellite repeats [2, 3]. When STR occurs within the 3% of the human genome known as protein coding/exon regions, they produce proteins critical for normal cellular functions. Additionally, these variations can contribute to pathologies arising from genetic modifications within exons. [2].

STR can be further classified into 2 types of repeats based on the number of repetitive sequences and the arrangement of these sequences with regard to one another. Simple uninterrupted repeats consist of one DNA sequence of a specific length repeated numerous times consecutively [4, 5]. When a simple microsatellite repeat has a non-repeat DNA sequence within the repeat region, the repeat is referred to as an interrupted or imperfect repeat [4]. A compound or composite repeat consists of various repetitive DNA sequences juxtaposed adjacent to one another in one reading frame [4].

When a particular STR's trinucleotide repeat sequence is amplified beyond the number of repeats normally found in the genome of a healthy individual, aberrant proteins are produced and lead to numerous neuropsychiatric and neuromuscular disease phenotypes [6-8]. As the trinucleotide repeat tract expands in length beyond the normal threshold, the probability of further expansion of the tract also increases in likelihood [7]. Consequently, the tract's expansion results in an earlier age of disease onset within generations as well as an increase in symptom severity. This hastening presentation of disease symptoms is termed anticipation [7, 9].

The molecular pathogenesis of trinucleotide repeat expansion diseases originates from loss-of-function (LOF) or gain-of-function (GOF) modifications within corresponding pathognomonic genes due to diminished or excessively produced protein [10, 11]. Diseases attributed to LOF include the neurodevelopmental fragile X disorders (FRAXA and FRAXE). In these diseases, LOF represses transcriptional activity leading to diminished gene products (10). In FRAXA, an expanded CGG repeat occurs at the fragile X A site within the 5' untranslated region (UTR) of the fragile X mental retardation 1 (*FMR1*) gene [8, 12]. FRAXE, Fragile X E mild mental retardation, patients also carry a CGG repeat at the FRAXE fragile chromosomal site, located approximately 600 kb distal to FRAXA [13].

GOF modifications are notably present in Huntington's disease (HD), Spinocerebellar Ataxia Type 1 (SCA1) and Oculopharyngeal muscular dystrophy (OPMD). HD contains a CAG repeat on chromosome 4 encoding the pathologic polyglutamine tract (polyQ) responsible for the pathognomonic Huntington protein [8, 14, 15]. SCA1 contains a CAG repeat on chromosome 6 [8, 16]. In OPMD, a GCG repeat encoding alanine (Ala) is observed within exon 1 of the polyA-binding protein nuclear 1 (*PABPN1*) gene when the number of repeats exceeds the normal 10 repeats [7].

Chapter 2: Literature Review

2.1 Mechanism of Repeat Formation

Trinucleotide repeat formation and subsequent expansion is attributed to the process of DNA slipped strand mispairing or replication slippage [17]. In this process, DNA polymerase encounters STR within the human genome during DNA replication or DNA repair and the enzyme detaches from the template DNA strand. DNA polymerase then reattaches to another portion of the repetitive sequences upstream of its original location at the time of detachment. When the DNA polymerase reinitiates activity, the STR region can be expanded [18, 19]. Importantly, as the expanded repeat region increases in size, the frequency of DNA slippage events also concurrently increases as well. The reason for this acceleration in further strand slippage is the formation of hairpin loops from single-stranded DNA's repetitive elements of the 4 nucleotides [19, 20]. Hairpin loops refer to regions of STR within the same DNA strand which fold and complementarily base pair with one another (A to T or C to G). Within these regions, STR are expanded as the DNA polymerase slips off the template strand when encountering a hairpin (stem loop) secondary structural conformation after nucleotides base pair and fold [20]. As the DNA polymerase resumes activity upon reattachment within another portion of the STR tract towards an end of the stem loop, the number of STR increases thereby enlarging the size of the expanded repeat tract [18]. This expansion of STR thus predisposes an individual to genetic anticipation in subsequent generations. This is due to the increased risk of future genetic modifications, as the potential for the creation for stabilized hairpin loops grows correspondingly [21, 22].

2.2 Oculopharyngeal Muscular Dystrophy (OPMD)

OPMD is a predominantly autosomal dominant progressive myopathy characterized by progressive drooping of the eyelids (ptosis), difficulty swallowing (dysphagia), weakness and atrophy of the tongue and proximal limb weakness [23, 24]. Other symptoms can also include impairment in speech function (dysarthrophonia) and aspiration pneumonia, which is one of the leading causes of mortality alongside malnutrition or starvation [25, 26]. Symptoms tend to initially present within the 5th to 6th decade of life [27]. Additionally, OPMD has an increased carrier allele frequency of 1/1000 within families of French-Canadian descent [28]. Unlike other trinucleotide repeat neurological diseases, anticipation due to STR expansion has not been observed but the average age of onset based on age of diagnosis is seen earlier in patients with larger expansions in the STR region causative for OPMD [24, 29]. Additionally, the symptoms of OPMD only manifest within voluntary muscles and have not been observed in smooth and cardiac muscles. Voluntary muscles affected bilaterally include levator palpebrae, the tongue, pharynx, extraocular muscles, gluteus maximus, deltoid and hamstrings [26]. In a clinical study of OPMD patients, Magnetic Resonance Imaging (MRI) determined that the individual muscles most severely compromised in particular were the tongue muscles, adductor magnus and soleus (a calf muscle) [30].

Tomé *et al* identified intranuclear inclusions (INI) within skeletal muscles characterized by the presence of tubular filaments within muscle fiber nuclei of OPMD patients [31]. Upon further examination of a cohort of 144 OPMD families who displayed INI within skeletal muscle fibers, the expansion of the Poly(A) binding protein nuclear 1 (*PABPN1*) gene was identified as the cause of OPMD [28]. Specifically, expansions of the sequence and to a lesser extent (GCG)_n which both encode alanine at exon 1 within the 5' end N-terminus region of *PABPN1* were

shown to be sufficient for the accumulation of misfolded PABPN1 protein as INI when the number of GCG repeats exceeds 10 triplets, typically in the range of 11-18 consecutive GCG repeats [7, 32].

PABPN1 is an ubiquitously expressed protein (32.8 kDA predicted and 50 kDA after post-transcriptional modifications) critical for mRNA stability and nuclear to ribosomal translocation via polyadenylation of nascent mRNA transcripts [23, 33, 34]. After transcription, mRNA transcripts undergo the addition of a poly(A) tail at the 3' end for stability and prevention of premature degradation prior to ribosomal translocation from the nucleus [34]. The wild-type *PABPN1* gene is composed of the various domains: a short alanine stretch, a proline rich region, an α -helical region, an RNA binding domain and a nuclear localization signal (NLS) [23]. In the mRNA polyadenylation reaction, the RNA binding domain of PABPN1 binds to the poly(A) tail of mRNA to efficiently catalyze the polyadenylation reaction of poly(A) polymerase which adds approximately 250 nucleotides to the 3' end of the mRNA transcript [35, 36]. The PABPN1 NLS is vital for OPMD pathogenesis as it has been shown to significantly contribute to INI observed in OPMD. When the mutant PABPN1 Ala-18 NLS was inactivated and a strong nuclear export sequence was fused to mutant PABPN1 in its place, Green Fluorescent Protein-tagged (GFP) PABPN1 demonstrated a resulting decrease in INI and cellular toxicity, which are the main molecular mechanisms responsible for OPMD disease formation and symptomatic progression [37].

2.3 OPMD treatment options

Despite advances made in understanding the pathogenesis of OPMD, there is no effective or curative treatment option available to patients [38]. There are only management strategies aimed at temporarily mitigating the negative effects of disease progression to provide a transient

improvement in quality of life. In particular, the most notable clinical symptoms of late-stage OPMD include dysphagia leading to aspiration pneumonia, ptosis significantly impairing vision and proximal limb weakness affecting mobility [38].

There are temporary non-curative surgical/non-surgical based strategies aimed at alleviating these symptoms. For dysphagia, a surgical option in the form of surgical cricopharyngeal myotomy is available to provide temporary relief for patients encountering difficulties swallowing when consuming food [39]. In this procedure the cricopharyngeal (CP) muscle which overlies the esophagus is essentially dilated or stretched surgically in order to aid in food passage and consumption [40]. Specifically, the constrictor muscles, through which food must initially bypass before encountering the CP, are weak thereby compromising the proper opening of the CP which normally ensures that food can proceed to the esophagus and the gastrointestinal tract as opposed to the trachea [40, 41]. If food erroneously enters the trachea due to CP weakness or uncoordinated peristalsis movements upon consumption, aspiration pneumonia is a severe consequence [38]. Despite the success of this CP procedure, patients often encounter a recurrence of dysphagia and the need for additional surgical procedures on the CP in the range of approximately 1-3 years post operatively [39].

The ptosis and subsequent compromised vision encountered by patients can be temporarily managed by blepharoplasty, a surgical procedure for the eyelids. Two forms of blepharoplasty can be performed in order to correct ptosis: levator palpebrae aponeurosis resection and frontal suspension of the eyelids [42]. Levator palpebrae resection, indicated as the primary corrective surgery, consists of shortening the levator palpebrae aponeurosis and reconnecting the levator palpebrae muscle to the tarsal plate of the upper eyelid [42, 43]. In this approach, a thread of muscle fascia is inserted through the tarsal plate of the upper eyelid and the

ends of the fascia are attached to the frontalis muscle [42]. While the levator palpebrae resection may need to be repeated once or twice, the frontal suspension procedure is permanent and done under anesthesia [42, 43].

Non-surgical therapeutic approaches have also been evaluated including chaperone proteins, small molecule inhibitors and intrabodies. In the case of chaperone proteins, the ubiquitin-proteasome pathway is essential to prevent the accumulation of misfolded polypeptides such as aggregates of PABPN1 INI observed in the histology of OPMD patient skeletal muscle biopsies [31, 44]. In particular, the chaperone proteins, heat shock protein 40 (HSP40) and heat shock protein 70 (HSP70), prevent aggregate formation of misfolded proteins and promote ubiquitination leading to prompt degradation of abnormal proteins to avoid cellular toxicity [45-47].

Several small molecule inhibitor strategies, including sirtinol (a histone deacetylase inhibitor), lithium chloride, valproic acid, and trehalose have also been examined *in vitro* within COS7 cells and lymphoblastoid cell lines derived from OPMD patients as well as *in vivo* within mouse and *C. elegans* models [48-51]. The main principal behind each of these strategies is to reduce the negative toxic effects of mutant PABPN1 Ala insoluble INI aggregates to avoid premature cellular apoptosis and compromised muscle functions [49, 50].

Another strategy developed by Verheesen *et al.* utilized a panel of multiple single-domain antibody reagents (VHH) which recognized different PABPN1 epitopes from endogenous PABPN1 within cell lysates and labeled PABPN1 within cell lines and muscle sections [52]. When VHH was expressed as modified intracellularly expressed antibodies targeting particular antigens in subcellular locations (intrabodies) in an OPMD cellular model, PABPN1 aggregation was inhibited in a dose-dependent manner and VHH also reduced pre-

existing PABPN1 aggregates [52, 53]. Within an *in vivo* Drosophila OPMD cell model, Llama single-chain intrabodies suppressed OPMD muscle degeneration, reduced PABPN1 aggregate formation and restored muscle gene expression [53].

A phase I/IIa clinical study (ClinicalTrials.gov [NCT00773227](https://clinicaltrials.gov/ct2/show/study/NCT00773227)) of 12 clinically and genetically diagnosed OPMD patients was conducted by Périé *et al.* to determine the safety and efficacy of autologous myoblast transplantation following myotomy [54]. Patients were evaluated via videoendoscopy and videofluoroscopy of swallowing and a quality of life score [54]. Following the transplant and up to 2 years post-transplant, no adverse effects were observed and all 12 patients experienced a cell dose-dependent improvement in quality of life with 10 patients indicating no functional degradation in swallowing capacity [54]. Despite the improvements observed in these approaches, patients experienced recurrence of symptoms due to the lack of correction of the root cause, which is the underlying genetic mutation responsible for disease formation and progression.

2.4 RNAi

Ribonucleic acid interference (RNAi) is a gene expression regulatory mechanism found within eukaryotic organisms utilizing small RNAs less than 30 base pairs long to complementarily bind and degrade sequence-specific mRNA transcripts leading to suppression of protein synthesis [55, 56]. Fire, Mello and colleagues established that double-stranded RNAs can activate RNAi to catalytically degrade complementary mRNA transcripts in *C. elegans* [57].

This seminal finding provided the key insights necessary for numerous downstream applications with regards to potential therapeutic options for human diseases. The RNAi pathway is operated by two groups of RNA: MicroRNA (miRNA) and small interfering RNA (siRNA). The key distinction in these two molecules lies in their origin, structure and specificity. miRNA

is endogenous within a cell, single-stranded with the capability to form hairpin loop structures and specific to multiple RNA target sequences [58, 59]. By contrast, siRNA are exogenous, 21-23 nucleotide RNA duplexes and specific to one RNA target sequence [58].

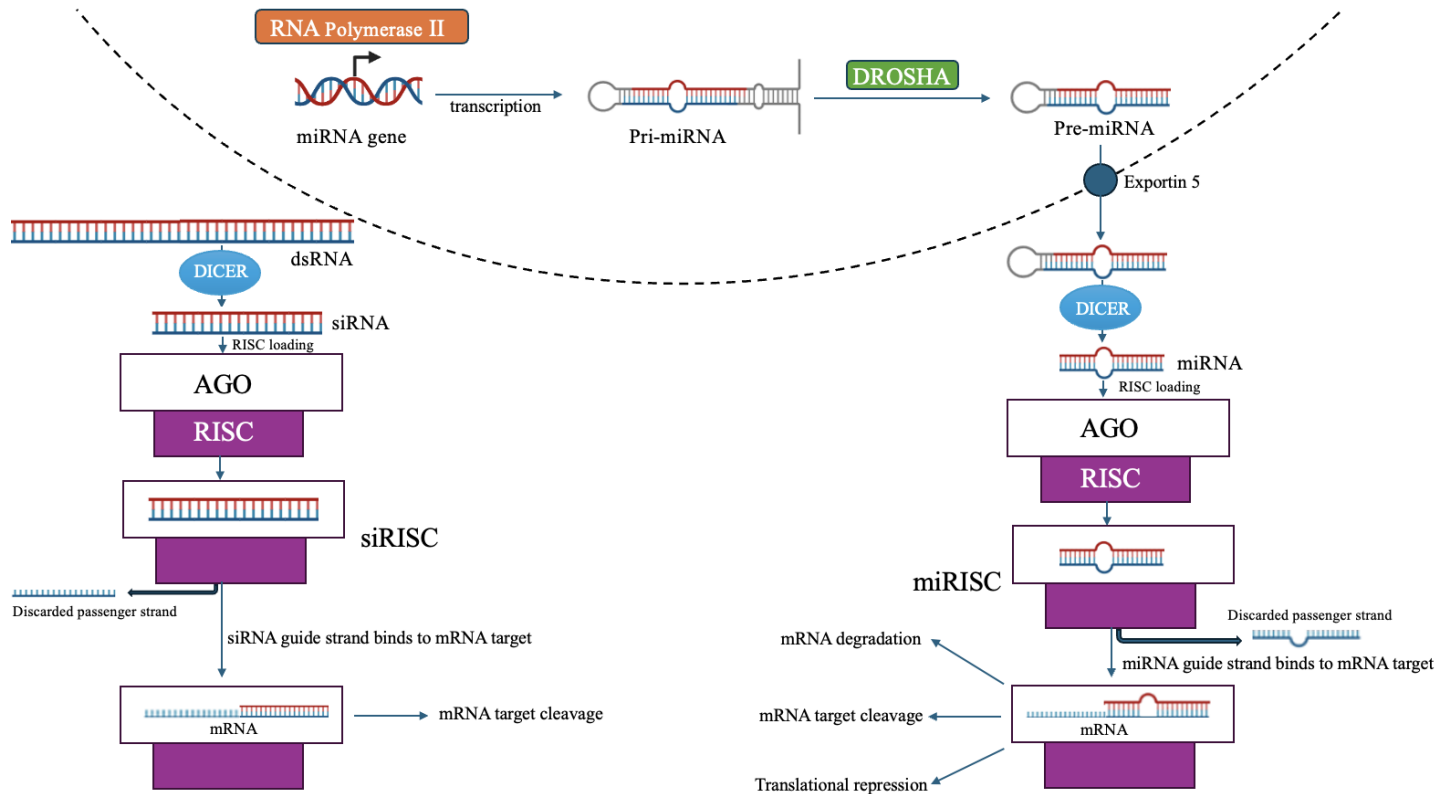


Figure 1. RNAi pathways of siRNA and miRNA

The RNAi pathway for miRNA gene silencing consists of a series of molecular interactions and enzymatic steps producing functional miRNA from primary precursor miRNA (pri-miRNA) (Figure 1) [60]. Initially, RNA Polymerase II produces pri-miRNA which is then processed by the DROSHA (nuclear RNase III) and DGCR8 protein complex [58, 60]. Next, Exportin 5 (Exp5) translocates the pre-miRNA from the nucleus to the cytoplasm for further processing in which DICER (Endoribonuclease RNase III) cleaves the stem loop region of the

hairpin formation forming a double stranded miRNA [58, 60]. Subsequently, the double stranded miRNA separates into two single stranded miRNAs and the miRNA complementary to the region of interest binds Argonaut (Ago) to form the RNA-Induced Silencing Complex (RISC) [58, 60]. At this point, the passenger miRNA strand is discarded and the miRNA RISC complex (miRISC) is led by the RNA guide strand to complementarily bind the target mRNA of interest producing translational repression and mRNA cleavage/degradation [58, 60].

2.5 RNAi Therapy in Monogenic and Trinucleotide Repeat Neurological Diseases

RNAi has shown promise as a potential targeted therapeutic option for neurological diseases including Duchenne's Muscular Dystrophy (DMD) and Spinal Muscle Atrophy (SMA). In DMD, there are mutations in the gene encoding dystrophin which produce an unstable or nonfunctional protein with resultant loss of muscle function [61]. Eteplirsen, an RNA-based oligonucleotide agent, causes skipping of a splice site within exon 51 in order to produce a shortened but functional dystrophin protein with a restored reading frame [61]. SMA is an autosomal recessive disease caused by nonsense or frameshift mutations in the *SMN1* gene leading to loss of SMN1 function and severe muscle weakness [61, 62]. Nusinersen acts on a site 3' of the boundary of exon 7 within the *SMN2* gene to induce exon switching to include exon 7 into SMN2 mRNA. This process ensures that there is an increase in the amount of full-length SMN2 to prevent complete SMN deficiency due to SMN1 mutation [61].

Additionally, there are examples of RNAi therapy for trinucleotide repeat diseases, specifically Machado-Joseph disease (MJD) and HD. Hu *et al.* demonstrated the use of peptide nucleic acid and locked nucleic acid antisense oligomers to target CAG repeats for the alleles of the ataxin-3 (*ATXN3*) and huntingtin (*HTT*) genes in MJD and HD [63]. This strategy successfully produced allele-specific silencing of the mutant alleles while not cleaving normal

mRNA [63, 64]. Thus, precedents exist to apply RNAi therapy approaches to OPMD, another trinucleotide repeat disease.

2.6 RNAi Therapy in OPMD

Malerba *et al.* demonstrated the use of an adeno-associated virus (AAV) based combinatorial approach of RNAi knockdown of endogenous PABPN1 (wild type) with simultaneous co-expression of sequence-optimized normal PABPN1 resistant to RNAi in order to prevent muscle degeneration in an OPMD mouse model [65]. In particular, dual therapy reduced the amount of insoluble PABPN1 aggregates, decreased muscle fibrosis and improved muscle strength to the level of healthy muscles [65]. When the RNAi knockdown and AAV approaches were tested individually, muscle degeneration persisted by comparison to improvement in muscle function observed in the dual therapy approach [65].

These findings were affirmed in our laboratory through an RNAi-based approach in C2C12 cell line and *C. elegans* OPMD models [38]. Selective miRNAs and hammerhead ribozymes (hhRzs) reduced the expression of wildtype and expanded repeat PABPN1 mRNA and protein levels by as much as 90% [38]. Due to miRNA's inability to distinguish between endogenous wildtype and mutant PABPN1, an optimized PABPN1 (optPABPN1) with a modified cDNA sequence also expressing PABPN1's alanine repeat sequence with GCA instead of GCG was applied [38]. This co-expression of optPABPN1 with miRNA knockdown of endogenous PABPN1 prevented cell death by restoring the level of wildtype PABPN1 [38].

2.7 Rationale and Objectives

Based on an evaluation of RNAi for OPMD models, there is a necessity to design an RNAi approach to avoid the consequences of cell toxicity and death as a result of indiscriminate wildtype and expanded repeat PABPN1 knockdown. As the miRNA-based knockdown approach

has been shown to effectively target PABPN1 in various OPMD models, it is a desirable approach to optimize to achieve discriminatory mutant PABPN1 knockdown. Thus, we hypothesize that designing modified PABPN1 microRNAs which only target the mutant PABPN1 GCG expanded allele while sparing the wildtype PABPN1 allele could achieve a desired treatment effect in OPMD. The objectives of this study are the following:

1. Design 12 miRNAs to specifically target the GCG expanded repeat mutant PABPN1 allele.
2. Clone miRNA 2 into a stable expression vector and transfect 2 OPMD cell lines expressing both wild type and expanded PABPN1: Human Embryonic Kidney Cells (HEK293T) and C2C12 murine myoblast cells.
3. Determine the optimal miRNA sequences which discriminately knockdown mutant PABPN1 without silencing wildtype PABPN1 based on western blot and RT-qPCR analyses of the efficacy and selectivity of the initially evaluated candidate miRNA 2.

Chapter 3: Materials and Methods

3.1 MiRNA Plasmid

Twelve miRNAs were designed to specifically target the mutant Ala-17 expanded repeat PABPN1 using the Invitrogen BLOCK-iT Pol II miR RNAi expression vector kit as per manufacturer's instructions. Key features of the pcDNA 6.2-GW/EmGFP-miR plasmid expression vector backbone include: a GFP tag to verify transfection efficiency and PABPN1 knockdown efficiency within cell lines, two separate 5' to 3' 4 nucleotide overhangs of ACGA and CAGG respectively, a robust Pol II human CMV (cytomegalovirus) promoter and a Spectinomycin resistance gene.

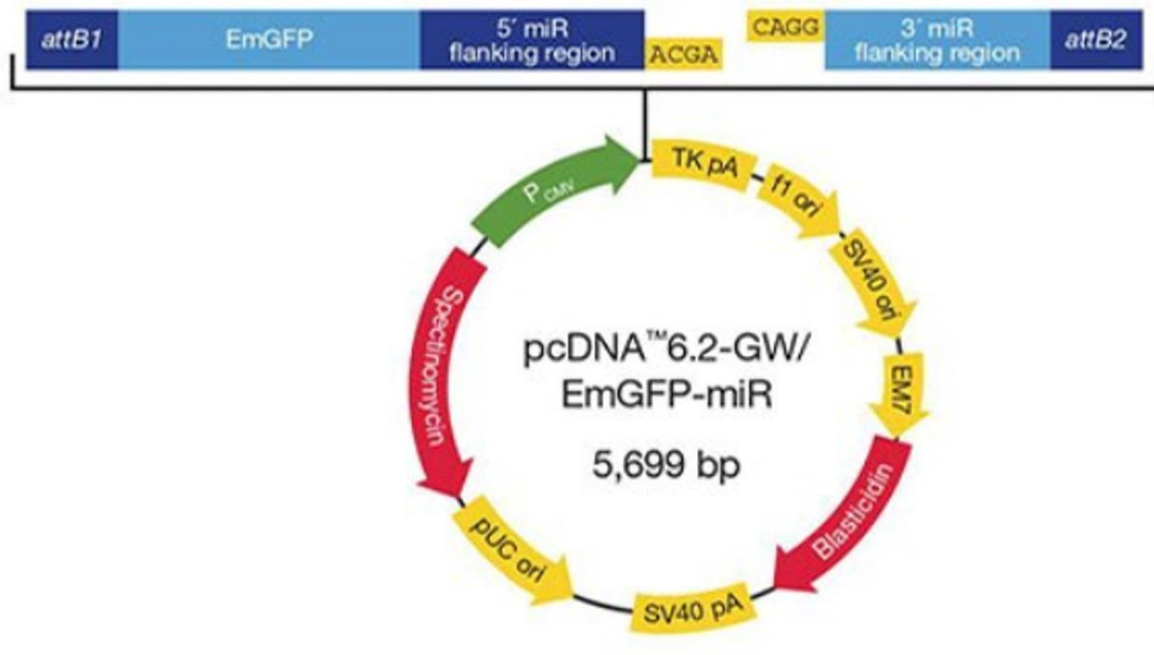


Figure 2. Invitrogen BLOCK-iT Pol II miR RNAi pcDNA GFP expression vector

Due to an insufficient amount of the pcDNA 6.2-GW/EmGFP-miR required for high volume miRNA cloning, enrichment of the plasmid was necessary prior to miRNA plasmid assembly and downstream applications. Thus, the open linear plasmid was closed with the

introduction of 2 single stranded DNA oligos each containing 2 5' to 3' 4 nucleotide complementary overhang regions and 2 Bsa1 restriction digest sites (Bsa1 linker F and Bsa1 linker R) (Figures 3 and 4).

Bsa1 linker F: TGCTCGAGACCACTGTAAAACGACGGCCAGTACTGGTCTCT

Bsa 1 linker R: CCTGAGAGACCAGTACTGGCCGTCGTTTTACAGTGGTCTCG

Figure 3. 5' to 3' Bsa1 forward and reverse single stranded linker oligos



Figure 4. Bsa1 restriction enzyme recognition site, restriction digest product and overhang

10uM of Bsa1 linkers F and R were added to IDT annealing (duplex) buffer at 95°C for 4 min with gradual $\Delta 10^\circ\text{C}$ until reaching room temperature. Next, the ligation reaction was performed with the double-stranded oligo, 10X T4 Ligase buffer, T4 DNA Ligase pcDNA emGFP vector and DNase/RNase free water as per manufacturer's protocol (Invitrogen). 5 ul of the ligation reaction product was then transformed into 25 ul of XL10 gold competent cells via heat shock transformation. Next, 50 ul of the transformation reaction product was streaked on LB agar plus Spectinomycin 100 mm x 15 mm petri dish plates with aseptic technique (flame on within close proximity to the plates during plate preparation and streaking colonies post transformation). The following day colonies were picked and inoculated in 3 ml LB plus 4 ul Spectinomycin on the 37°C shaking incubator. Consequently, after centrifuging the tubes, a pellet was collected, and midi-prep was performed using the Qiagen QIAprep spin miniprep kit as per manufacturer's instructions. Following this step, the validity of the cloned constructs was confirmed by Sanger sequencing at the McGill Genome Centre prior to downstream applications.

3.2 MiRNA Constructs

Twelve miRNA constructs were designed as double stranded oligos containing certain elements necessary to target the desired GCG trinucleotide expanded repeat found in OPMD. Due to a provisional patent pending, specific information regarding the miRNA constructs, such as their ID numbers, sequences, target regions and modifications to improve selectivity, cannot be presently depicted. Each of the twelve constructs contain a TGCT 5' overhang complementary to the plasmid (for directional cloning) followed by a 5'G nucleotide. There are also short 21 nucleotide antisense sequences which bind the target region of the expanded GCG trinucleotide repeat. Additionally, a 19 nucleotides short spacer forms the terminal loop which is ultimately removed during miRNA processing and a sense target sequence of PABPN1 is present at nucleotides 1-8 and 11-21. In certain constructs, nucleotides (nts) 9 and 10 were removed from the passenger (p) and guide (g) strands for the creation of an optimized internal loop structure. The two nucleotides internal loops were chosen due to a higher relative knockdown rate compared to the 3 or 5 nucleotide internal loops counter parts.

Six miRNAs were constructed with this template and an additional six miRNA constructs were designed similarly except for the modifications of nucleotides 9 and 10 of the sense target sequence/guide strand to an A or T respectively. The introduction of these mismatch modifications have been shown to enhance the release of guide RNA from Ago 2 within the RISC complex which leads to more potent silencing of abundant mRNAs [66, 67]. Lastly, the constructs all contained a 5' to 3' CCTG overhang on the bottom strand.

These constructs were designed to target the *PABPN1* GCG repeat at various proximal and internal regions to determine the optimal miRNA sequences. The 3 targeted sites included areas adjacent (left or right) or centrally within the microsatellite repeat as shown in Figure 5.

5'-GGGCGGCGGGCCCCAGTCTGAGCGGGCATGGCGGGCGGGCGGGCGGGCGGGCGGGCGGGCGGCAGCAGCAGCGGGGGGCTGCG-3'
 5'-GGGCGGCGGGCCCCAGTCTGAGCGGGCATGGCGGGCGGGCGGGCGGGCGGGCGGGCGGGCGGCAGCAGCAGCGGGGGGCTGCG-3'
 5'-GGGCGGCGGGCCCCAGTCTGAGCGGGCATGGCGGGCGGGCGGGCGGGCGGGCGGGCGGGCGGCAGCAGCAGCGGGGGGCTGCG-3'

Figure 5. *PABPN1* ATG start codon (red), GCG repeat tract (yellow) and miRNA target region (underline)

The set of 12 miRNA ds oligos were then cloned into the 5,699 base pair pcDNA 6.2-GW/EmGFP-miR plasmid expression vector. Next, the cloned constructs of miRNA 1 and 2 were transformed, colonies were picked and midiprep was performed following the procedure used to enrich the pcDNA 6.2-GW/EmGFP-miR plasmid. The identities of the cloned sequences were also verified by Sanger sequencing at the McGill Genome Centre using the following plasmid sequencing primers: 5'-GGCATGGACGAGCTGTACAA-3' (forward sequencing primer) and 5'-CTCTAGATCAACCACTTTGT-3' (reverse sequencing primer) (Figure 6).

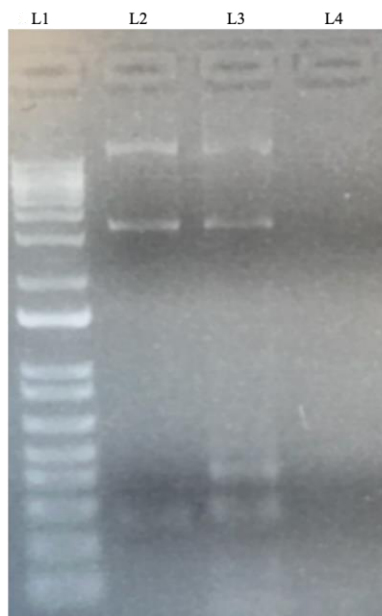


Figure 6. 1% agarose DNA gel: Lane 1 (L1)-1 kb plus ladder, L2- miRNA1, L3- miRNA2, L4- negative control

MiRNAs 1 and 2 were selected as the initial candidates for evaluation due to their designs targeting the *PABPN1* repeat at the regions left adjacent and centrally within the repeat without further modifications to enhance selectivity. MiRNA 2 was further prioritized for

evaluation over miRNA 1 due to its ability to target the region left adjacent to the ATG start codon and GCG expanded repeat tract. As these regions include the promoter and promoter-associated elements which regulate PABPN1 expression, the capacity of miRNA 2 to target and disrupt these regions in theory gave credence to its selection as the first candidate to be evaluated amongst all miRNA constructs.

3.3 PABPN1 Ala-10/17 Dsred Plasmids

The cDNA of *PABPN1* wildtype Ala-10 and mutant allele Ala-17 were subcloned into a Dsred vector thereby producing an Ala-10/17-RFP fusion product encoding PABPN1 Ala 10 and 17 tagged with Red Fluorescent Protein (RFP). The PABPN1-Dsred vectors were synthesized based on prior OPMD studies conducted by the Rouleau group [38, 49, 68, 69]. The value of this GFP and RFP approach was to evaluate miRNA knockdown of endogenous and external wildtype (Ala-10) and mutant (Ala-17) forms of PABPN1 during co-transfection of both GFP and Dsred vectors in HEK293T and C2C12 cells. The distinguishing colors enabled the verification of transfection, estimation of transfection efficiency and the visual imaging of miRNA-induced PABPN1 knockdown prior to protein and RNA analyses.

3.4 MiRNA transfection into HEK293T and C2C12 cells

Following the verification of miRNA constructs' identities, the subcloned miRNA-GFP and PABPN1-Dsred constructs were transfected into Human Embryonic Kidney Cells (HEK293T) and C2C12 murine myoblast cells in order to assess PABPN1 knockdown *in vitro*. The cell lines were obtained from the previous work done by the Rouleau laboratory with regards to OPMD [38, 49, 50]. HEK293T and C2C12 cells were obtained from liquid nitrogen stocks and cultured in 100 mm x 15 mm petri dishes containing 10 ml of DMEM (Invitrogen) with 10% and 20% fetal bovine serum (fbs) respectively. The cells were initially grown as a

monolayer at 37°C with 5% CO₂ in cell culture incubators. When the cells reached a 70%-80% confluence after a minimum of two passages, the cells were washed with Dulbecco's Phosphate-Buffered Saline (DPBS) then detached with 1% trypsin and seeded at a density of 1x10⁵ cells/ml in 12-well plates (1 ml final volume) 24 hours prior to transfection. HEK293T cells were transfected with 1 µg of DNA consisting of miRNA 2 and PABPN1 plasmids using the Jet prime transfection reagent (Polyplus) following the manufacturer's instructions. Additionally, miRNA 7-2 tagged with GFP (positive control) was transfected simultaneously with the same transfection reagent due to prior use indicating its high transfection efficiency and PABPN1 knockdown capability. Transfections were done in triplicate with parallel plates for each experiment after which protein and RNA extractions were performed. A representative 12-well transfection plate using the Jet prime transfection reagent is shown in Figure 7.

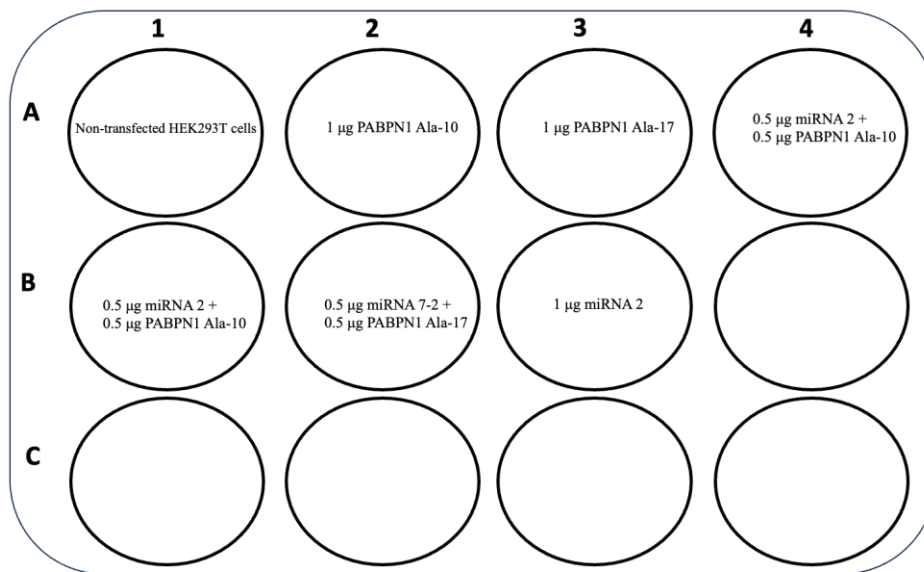


Figure 7. HEK293T 12-well plate transfection layout with 1 µg of plasmid DNA (Jet prime)

C2C12 cells were initially transfected with 1 µg of DNA with the Jet prime transfection reagent in the same manner as the procedure for HEK293T cells but the transfection efficiency was poor upon GFP and RFP visualization 48-72 hours post transfection. Therefore, the

Lipofectamine 2000 (Invitrogen) transfection reagent was alternatively used for C2C12 transfection following the manufacturer's protocol. 0.5×10^5 cells/ml were seeded in 12-well plates overnight and transfected with 0.8 μg of plasmid (GFP and RFP) DNA.

3.5 Fluorescence microscopy

Transfection efficiency and cell viability were determined 48-72 hours post transfection with the EVOS fluorescence microscope (Invitrogen). Numerous images were captured in the phase, GFP and Dsred channels of each well. The presence of GFP and Dsred fluorescence in their respective channels provided a visual approximation of transfection efficiency. After visually confirming that transfection was successfully achieved, protein and RNA were extracted from HEK293T and C2C12 cells to determine the extent of miRNA-induced PABPN1 knockdown.

3.6 Protein Extraction

Cells were scraped with pipette tips from each well of the 12-well plates 48-72 hours post transfection in the biosafety cabinet and placed on ice in Eppendorf tubes. The tubes were centrifuged for 5 minutes at 6,000 rpm in a cold setting and the supernatant was removed. The pellets were resuspended in 300 μl of PBS and centrifuged for 5 minutes at 6,000 rpm. 60 μl of the sodium sulfate utilizing buffer (SUB) reagent consisting of 0.5% SDS, 8M urea and 2% β -mercaptoethanol was added to each sample and mixed until the resuspension solution was dense and viscous. The mixed protein and SUB solution samples were placed for 2-3 minutes onto a preheated 400°C heat block containing boiling water and then transferred onto ice. The samples were stored in -20°C for storage. Prior to usage in western blot, the proteins were sonicated for 3 seconds, 3 times each on the 20 amps setting with ethanol sterilization of the sonication apparatus between each sample. After sonication, the protein concentrations were determined on

the spectrophotometer with the colorimetric standard Bradford protein assay (Bio-Rad protein assay dye) using Bovine Serum Albumin (BSA) as the metric for the standard curve.

3.7 RNA Extraction

The RNA extraction steps were completed in the biosafety hood in a sterile environment with autoclaved pipette tips and clean pipettes (RNAase Zap, Invitrogen) to avoid RNAse contamination. 300 μ l of TRIzol reagent (Invitrogen) was added to each well of the 12-well plates 48-72 hours post transfection and the contents were collected in Eppendorf tubes once the solutions were viscous. 70 μ l of chloroform was added to separate the homogenate into an upper clear aqueous layer with RNA, an interphase and a lower red organic layer with DNA and proteins. The solution was then vortexed vigorously for 15 seconds and incubated for 2 to 3 minutes in the biosafety cabinet at room temperature. In order to separate the layers for RNA collection, the samples were centrifuged at 12,000 rpm for 15 minutes in a cold setting. The clear upper aqueous layer with RNA was extracted, the RNA was precipitated with 150 μ l of isopropyl alcohol and the mixed solutions were incubated for 10 minutes at room temperature (for higher RNA yield the samples can also be precipitated in -20°C overnight).

Next, the samples were centrifuged at 12,000 rpm for 10 minutes in a cold setting. The supernatant was discarded, the RNA was washed with 300 μ l of 75% ethanol and the samples were stored in -80°C overnight. The following day the samples were centrifuged at 12,000 rpm for 5 minutes in a cold setting. After removing the ethanol, another wash of the RNA was done with 300 μ l of 75% ethanol, the ethanol was removed and the Eppendorf tubes with samples were left with caps open for 10 minutes to ensure the elimination of any excess residual ethanol. The RNA samples were dissolved in 18 μ l diethyl pyrocarbonate (DEPC), RNAse-free water and stored at -80°C .

3.8 Western Blot

10% polyacrylamide gels were prepared with the TGX FastCast acrylamide kit (Bio-Rad) and 1.5 mm Bio-Rad glass plates following the manufacturer's protocol. After performing the Bradford protein assay, an equal amount of protein samples (20 µg) were loaded into each well of the polyacrylamide gel. Additionally, 10 µl of the Precision Plus Protein Kaleidoscope Prestained Protein Standard (Bio-Rad) was loaded to determine the size of electrophoresed protein products. After adding the running buffer to the western blot apparatus, 85 V was applied for the initial 10 minutes of the gel run then increased to 100 V for the final 50 minutes of the run.

To transfer the proteins onto a nitrocellulose membrane, the Trans-Blot Turbo Transfer System (Bio-Rad) was utilized. The nitrocellulose membrane was prepared for the transfer procedure with the applications of ethanol and transfer buffer for 1 minute each respectively. The electrophoresed gel was placed on top of the nitrocellulose membrane with both components then surrounded by stacks of filter papers facing the anode (+) and cathode (-) areas of the transfer apparatus. Once the filter paper, gel and nitrocellulose membrane were firmly secured in place, 25 V was applied for 30 minutes to complete the wet transfer.

The nitrocellulose membranes containing the transferred protein products were blocked for 2 hours at room temperature in 10 ml of 5% milk resuspended in PBS-Tween (2.5 g baby milk diluted in 50 ml PBS-Tween) on a shaking incubator. Next, the milk was discarded, and the following primary antibodies were applied in 5 ml of 5% milk for an overnight incubation with agitation in a cold setting: PABPN1 rabbit monoclonal antibody (Abcam EP3000Y) (1:2500) and Actin mouse monoclonal C4 antibody (Merck Millipore MAB1501) (1:1000). After the primary antibodies with milk were removed, the blots were washed 3 consecutive times with 10 ml PBS-

Tween on a shaking incubator. 0.5 μ l of the following set of secondary antibodies diluted in 5% milk were applied to the blots: PABPN1 horseradish peroxidase-conjugated (HRP) goat anti-rabbit (ThermoFisher) (1:1000) and Actin HRP-conjugated horse anti-mouse IgG antibody (Cell Signaling Technology) (1:1000). The blots with secondary antibodies were incubated with agitation in a cold setting for 1 hour and then visualized with the Clarity Western ECL Substrate (Bio-Rad) and the ChemiDoc Imaging System (Bio-Rad). Images of the protein samples in the stained blots were taken at various exposure times in the chemiluminescence setting.

The densities of the visualized protein bands were quantified and analyzed with the ImageJ image analysis software (NIH) using actin as the loading control to normalize the relative protein content for each sample. Band densities were calculated by measuring the 8-bit (0-255) pixel intensity display values of each band in a constant and defined area. The results displayed in ImageJ consisted of the mean, minimum and maximum pixel intensities in the chosen area. Then, the mean intensities of actin bands were divided by the mean intensities of PABPN1 Ala-10/17 bands to determine the relative PABPN1 Ala-10/17 protein expression for each sample. This method uses actin as the loading control to correct for any unequal loading variation between the lanes. Also, mean actin intensity was divided by mean PABPN1 intensity due to the meaning of the pixel intensity display values in 8-bit for ImageJ. The measured values closer to 0 corresponded to darker areas on the gel which had a higher relative protein density and the measured values closer to 255 were brighter with a lower relative protein density. Hence, the lower pixel intensities represented a higher relative amount of protein after correcting for normalization with actin.

3.9 Quantitative RT-PCR

The SuperScript Vilo cDNA Synthesis Kit (Invitrogen) was used to produce cDNA from RNA samples with a concentration of 0.1 µg/µl per 10 µl total reaction volume following the manufacturer's protocol. cDNA samples generated were mixed with the *PABPN1* probe 5'-TCGAGGGTGACCCGGGGGA-3' (Applied Biosystems) and TaqMan Fast Advanced Master Mix (Applied Biosystems) in triplicate in 384 well 0.1 ml plates based on the manufacturer's instructions. The RNA polymerase II (RNAP) (Applied Biosystems, POLR2A- 4331182) probe 5'-GGGGCGGCCTCCCTCAGTCGTCTCTGGGTATTTGATGCCACCCTCCGTCACAGACATTTCGC-3' served as the internal control to normalize any variations in the data based on differences in experimental conditions (unequal loading of proteins in different lanes). RNAP was selected as the reference gene due to its ubiquitous expression in all tissues irrespective of differences in the amount of genetic material and experimental factors [70]. qPCR experiments were performed at 50°C for 2 min, 95°C for 20s and 40 cycles of 95°C for 1s and 60°C for 20s.

RT-qPCR was completed with the QuantStudio Real-time PCR system (Applied Biosystems) and the data was evaluated with the QuantStudio Real-time PCR software (Applied Biosystems). The comparative CT method ($\Delta\Delta CT$) was used to determine the relative quantification of mRNA. In this method, the cycle threshold (CT) value corresponds to the number of reaction cycles required to detect fluorescence signal beyond a predetermined baseline detection threshold accounting for background fluorescence [71]. The CT values are inversely related to the starting amount of cDNA in the qPCR reaction. A lower CT value thus equates to a higher initial amount of cDNA and vice versa.

The CT values for the target gene and the housekeeping reference gene were determined for each of the samples and controls. The 4 CT values were then normalized by taking the

differences in PABPN1 CT values and the RNAP CT values ($\Delta\text{CT} = \text{PABPN1 CT} - \text{RNAP CT}$) for each of the treated samples and controls. Since the qPCR experiments were done in triplicates, averages of the CT values were calculated for the samples and controls. Consequently, the $\Delta\Delta\text{CT}$ values were calculated by determining the difference in the ΔCT values of the samples and control ($\Delta\Delta\text{CT} = \text{Sample } \Delta\text{CT} - \text{Control } \Delta\text{CT}$). The relative quantification (RQ) of gene expression fold change between the samples and control was calculated by taking $2^{-\Delta\Delta\text{CT}}$. The RQ values were plotted to show the comparative changes in relative gene expression to the RQ control value of 1 (100% PABPN1 expression) for PABPN1 Ala-10. Thus, the RQ values on the plot show the relative differences in PABPN1 gene expression after miRNA treatment (miRNA 2).

Chapter 4: Results

4.1 Fluorescent Imaging of HEK293T and C2C12 transfected cells

HEK293T and C2C12 cells were each transfected with miRNA 2, PABPN1 Ala-10 (wildtype), PABPN1 Ala-17 and miRNA 7-2 (known positive control due to effective PABPN1 knockdown in previous studies). MiRNA2 and miRNA 7-2 were each tagged with GFP and the PABPN1 Ala-10 and Ala-17 were both tagged with DsRed (RFP). 48-72 hours post transfection images were taken of all transfected cells in the green and red channels respectively prior to obtaining protein and RNA for PABPN1 knockdown analysis. Multiple images were captured in each channel to represent different fields per well of the 12-well transfection plate. This approach was taken to ensure an accurate visual representation of the variable transfection efficiencies because certain areas of the transfected wells had larger aggregations of cells as opposed to a proper monolayer, uniform distribution of cells present during the initial seeding of cells before transfection. Additionally, as shown in Figure 8, capturing multiple fields of images provided a gross visual approximation of post transfection cell viability due to the previously established deleterious effect of PABPN Ala-17 on earlier cell death compared to cells expressing wildtype PABPN1 Ala-10 [72].

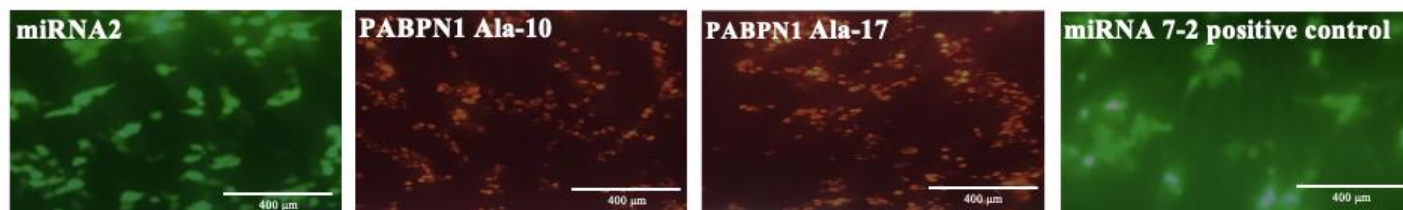


Figure 8. miRNA 2, PABPN1 Ala-10/17 and miRNA 7-2 in HEK293T cells 48-72 hours post transfection

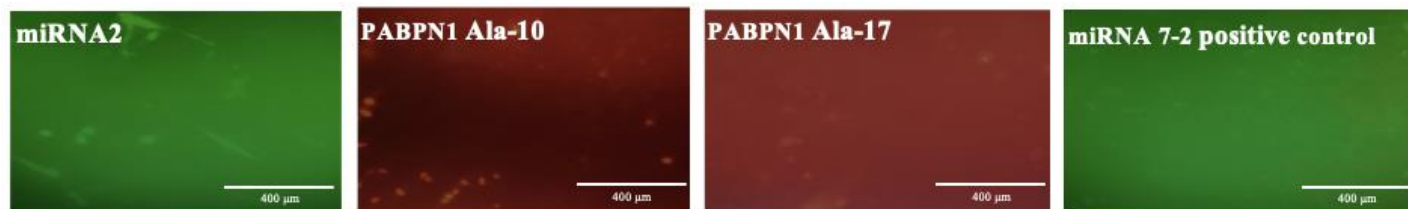


Figure 9. miRNA 2, PABPN1 Ala-10/17 and miRNA 7-2 in C2C12 cells 48-72 hours post transfection

The green channel depicted the transfection efficiency for the miRNA constructs and the red channel showed the transfection efficiency for the PABPN1 Ala-10/17 constructs. For both cell lines, it was imperative to ensure efficient transfection to properly analyze PABPN1 knockdown through the quantification of protein and RNA. Initially, HEK293T and C2C12 cells were both transfected with the Jet prime transfection reagent (Polyplus) but the C2C12 cells showed poor miRNA and PABPN1 Ala-10/17 transfection efficiency compared to HEK293T cells. Due to this discrepancy, the C2C12 cells were transfected using Lipofectamine 2000 (Invitrogen) (Figure 9). Despite the change in the transfection method, C2C12 cells showed a visibly diminished transfection efficiency for miRNA 2, PABPN1 Ala-10/17 and miRNA 7-2 positive control compared to transfected HEK293T cells.

4.2 Western blot of miRNA 2-induced PABPN1 knockdown in HEK293T

Western blot analysis of miRNA 2 and PABPN1 ala-10/17 transfected HEK293T cells was completed after fluorescent imaging, sonification of extracted proteins collected 48-72 hours post transfection and standard Bradford assay to calculate the concentration of total protein in each sample. The proteins were electrophoresed on SDS page gels to separate contents based on molecular weight and then transferred to a nitrocellulose membrane. The membrane was then stained with antibodies specific to PABPN1 and actin. Actin was chosen as the normalization control to ensure the potential effect of PABPN1 ala-10/17 knockdown was a result of miRNA

silencing as opposed to unequal protein loading in the various lanes of the SDS page gel. Actin is suitable as it is constitutively expressed in various tissues at levels of independent of any modifications in experimental conditions (housekeeping gene) [73].

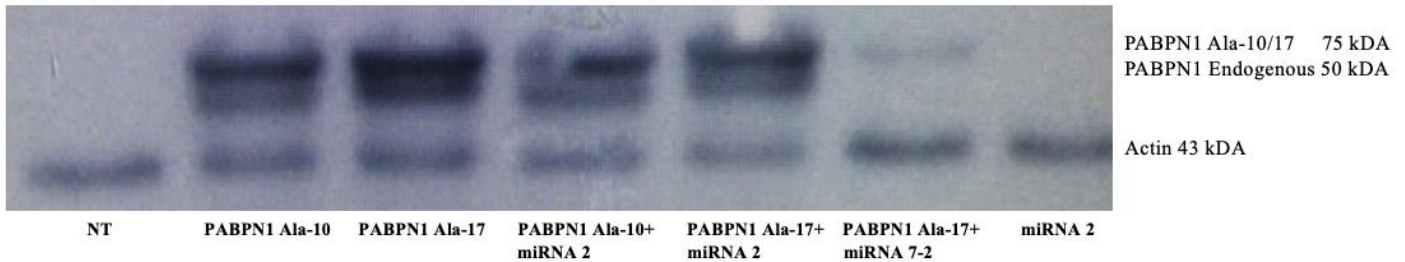


Figure 10. Western blot of miRNA 2-induced PABPN1 knockdown in HEK293T cells

An image of the blot probed for PABPN1 and actin proteins was taken (Figure 10). The bands on the image represent the amount of PABPN1 ala-10/17 (75 kDA), endogenous PABPN1 (50 kDA) and actin (43 kDA) proteins present at the time of extraction post transfection (48-72 hours). The endogenous PABPN1 was only present in lanes 2, 3, 4 and 5 of the gel.

Additionally, lanes 1, 6 and 7 of the gel represented the experimental controls. In lane 6 miRNA 7-2 served as a positive control due to its previously established function as an effective agent for PABPN1 ala-17 knockdown. Lanes 1 and 7 corresponded to the negative controls which were cells not transfected (NT) and cells only transfected with miRNA 2 without PABPN1 ala-10/17. Thus, the expected absence of PABPN1 ala-10/17 bands at 75 kDA in these lanes demonstrated the difference between treated and untreated samples.

To quantitatively assess the impact of miRNA 2-induced suppression on PABPN1 protein levels, densitometry analysis of the bands was performed using ImageJ. This analysis allowed for the determination of the relative amount of PABPN1 protein in both treated and untreated samples. Because the measured pixel intensities of each band were calculated in the 8-bit setting, a higher abundance in the quantity of relative protein present corresponded to lower

pixel intensities with the area of measurement kept constant between samples and proteins.

Consequently, normalization was done by dividing the mean values of actin controls by the mean values of PABPN1 Ala-10/17. All of the measured pixel intensities for the bands present and the normalized relative PABPN1 Ala-10/17 values are depicted below in Table 1.

Sample	PABPN1 Ala-10/17				Actin				Actin / (PABPN1 Ala-10/17)
	Area	Mean	Min	Max	Area	Mean	Min	Max	Normalization
PABPN1 Ala-10	637	58.71	38	96	637	106.684	91	127	1.81713507
PABPN1 Ala-17	637	46.604	28	88	637	101.215	86	120	2.17180929
PABPN1 Ala-10 + miRNA 2	637	66.848	43	105	637	116.983	101	137	1.74998504
PABPN1 Ala-17 + miRNA 2	637	67.642	43	114	637	125.885	111	145	1.86104787
PABPN1 Ala-17 + miRNA 7-2	637	150.13	133	164	637	108.779	91	136	0.72456538

Table 1. HEK293T miRNA 2-induced PABPN1 Ala-10/17 knockdown western blot densitometry calculations

The effect of miRNA 2-induced knockdown on PABPN1 Ala-10 levels relative to PABPN1 Ala-17 was examined as the aim of this study was to design and evaluate miRNA constructs specific and more selective to PABPN1 Ala-17 compared to PABPN Ala-10. The amounts of PABPN1 Ala-10/17 in the lanes not treated with miRNA 2 were chosen as the 100% reference point for comparative miRNA 2 PABPN1 Ala-10/17 knockdown analysis as depicted below in Figures 11 and 12.

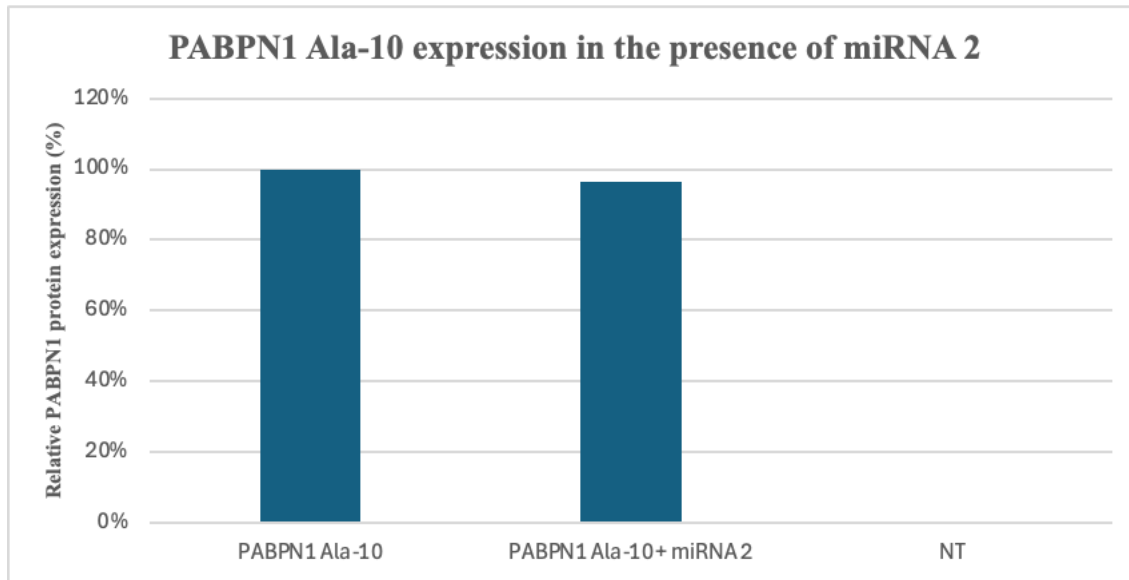


Figure 11. Relative PABPN1 Ala-10 expression after miRNA 2-induced knockdown

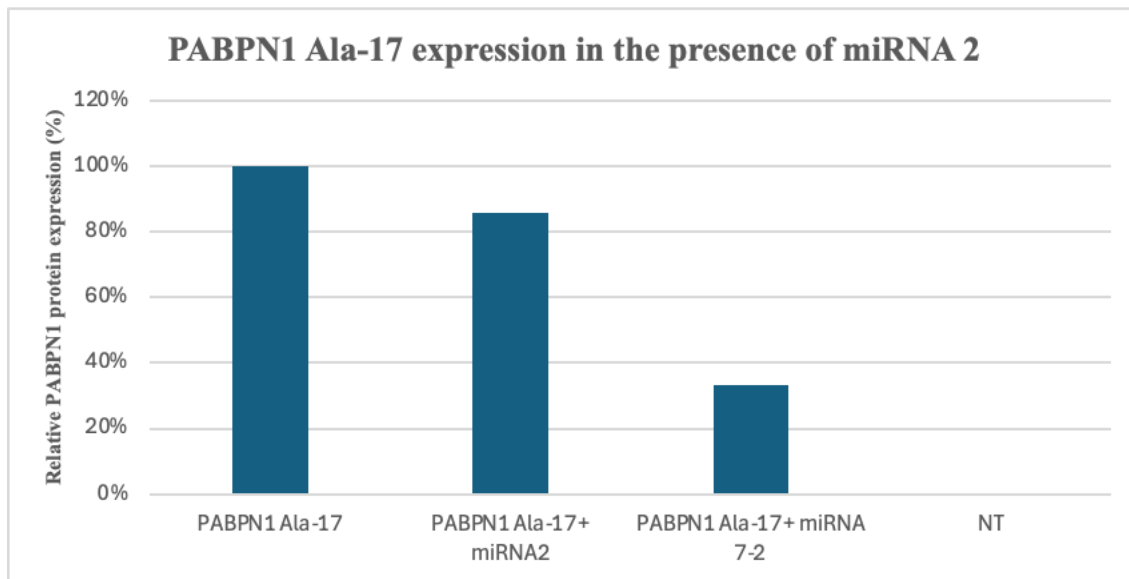


Figure 12. Relative PABPN1 Ala-17 expression after miRNA 2-induced knockdown

These findings indicate that the effect of miRNA 2 on PABPN1 Ala-10/17 knockdown is specific but not completely selective to the mutant form of PABPN1. Specifically, there is an approximately 4% reduction in PABPN1 Ala-10 treated with miRNA 2 compared to an approximately 14% reduction in PABPN1 Ala-17 (67% reduction in PABPN1 Ala-17 observed

for miRNA 7-2 positive control). While this result is not ideal in terms of completely selective PABPN1 Ala-17 knockdown, it does provide preliminary evidence in one cell line model (HEK293T) to suggest a slightly elevated level of PABPN1 Ala-17 knockdown compared to the wildtype PABPN1 Ala-10. Further testing evaluating miRNA 2 (tested only once in one cell line) as well as the other designed miRNA constructs with biological and technical replicates is necessary in order to establish a clear and statistically significant pattern of selective miRNA-induced PABPN1 knockdown.

4.3 RT-qPCR of miRNA 2-induced PABPN1 knockdown in HEK293T

RNA extraction was also performed concurrently on the HEK293T PABPN1 Ala-10/17 and miRNA 2 transfected cells. RQ represents a fold change in the relative amount of PABPN1 transcript expressed compared to the RQ value of 1 for the calibrator sample of PABPN1 Ala-10. The relative expression of PABPN1 levels is depicted below in Figure 13.

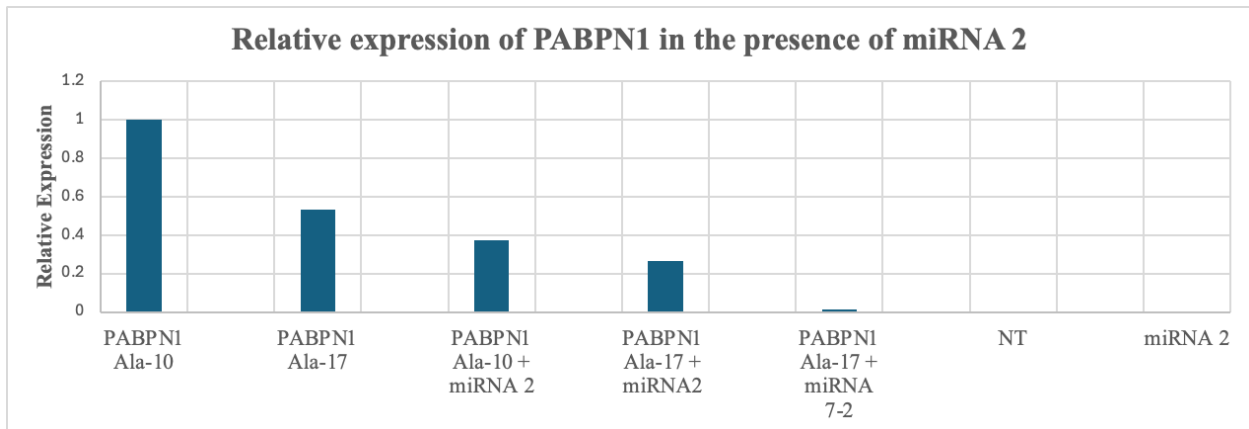


Figure 13. RT-qPCR of relative PABPN1 expression after miRNA 2-induced knockdown

There is an approximately 63% reduction in the relative expression of PABPN1 Ala-10 in the presence of miRNA 2 compared to PABPN1 Ala-10. Also, there is an approximately 50% reduction in the relative expression of PABPN1 Ala-17 in the presence of miRNA 2 compared to

PABPN1 Ala-17. Similar to the western blot result, miRNA 2 is specific but not completely selective in the discrimination of PABPN1 Ala-10 and PABPN1 Ala-17 during knockdown as both PABPN1 Ala-10 and PABPN1 Ala-17 transcripts are relatively reduced in the presence of miRNA 2. As expected, the non-transfected and miRNA 2 without PABPN1 Ala-10/17 samples showed no detection of PABPN1 expression while the PABPN1 Ala-17 + miRNA 7-2 positive control sample showed an approximately 98% reduction in PABPN1 Ala-17 expression. These findings are not concordant with the western blot analysis in which there was a slightly higher reduction in PABPN1 Ala-17 compared to PABPN1 Ala-10 due to miRNA 2 silencing. As was the case with the western blot, further rigorous testing with more replicates is imperative in order to definitively elucidate the effect of miRNA on relative PABPN1 Ala-10 and PABPN1 Ala-17 expression as the experiment was only performed one time.

Chapter 5: Discussion

5.1 miRNA effectively silences PABPN1 Ala-10/17 at the protein and RNA levels

The identification of trinucleotide expanded repeats within the *PABPN1* gene leading to intranuclear inclusions within skeletal muscles has been well established as the molecular basis for the cause of the autosomal recessive form of OPMD [28, 31, 32]. As the GCG_n *PABPN1* trinucleotide repeat expands in size, disease symptoms occur at an earlier age with elevated severity (anticipation) [24, 29]. Although the etiology of OPMD is monogenic, no effective curative therapeutic option is available for patients.

Current surgical and non-surgical strategies are only aimed at mitigating disease symptoms to improve quality of life to avoid late-stage complications [38]. Cricopharyngeal myotomy (stretching) provides temporary improvement in dysphagia-related symptoms and non-surgical options which have been investigated include chaperone proteins, small molecule inhibitors, intrabodies and myoblast skeletal muscle stem cell transplantation (ongoing clinical trials) [45, 48-50, 52-54]. Despite these limited treatment options, OPMD symptoms tend to reappear in an aggravated manner as the disease progresses. Thus, the absence of an effective treatment option is evident.

Findings from previous studies provided the basis for applying RNAi in the treatment of the mutant, disease-causing form of PABPN1 in OPMD. Prior approaches utilized miRNA and hammerhead ribozymes approaches to attempt to target PABPN1 in C2C12 and *C.elegans* OPMD models [38, 65]. However, in both studies miRNA constructs were not able to selectively discriminate wildtype from mutant forms of PABPN1.

As a result of these findings, the principal aims of this study were to design and evaluate the efficacy of miRNA constructs which selectively target the GCG_n expanded *PABPN1* repeat

without affecting wildtype PABPN1 in cell lines. The effectiveness of miRNA 2-induced PABPN1 knockdown at the protein and RNA levels was quantitatively determined by western blot and RT-qPCR analyses. Although twelve miRNA constructs were created, the initial candidate which was tested for effective and selective PABPN1 Ala-17 knockdown capability was miRNA 2. MiRNA 2 was chosen to establish a proof of concept for the reasons outlined above prior to evaluating the other candidates which possessed design modifications. In theory, these miRNA constructs have an enhanced selectivity towards PABPN1 Ala-17 based on the creation of an optimized internal loop structure due to modifications to specific nucleotides on the passenger and guide strands [74]. Preliminary western blot data of miRNA 2-induced PABPN1 Ala-10/17 knockdown in HEK293T cells showed a 14% reduction in PABPN1 Ala-17 compared to a 4% reduction in PABPN1 Ala-10 as a result of the miRNA 2-induced PABPN1 silencing. This finding varied from the RT-qPCR data which showed a 50% reduction in PABPN1 Ala-17 compared to a 67% reduction of PABPN1 Ala-10.

5.2 Study limitations

The primary difficulty with meaningfully interpreting the extent of effective and selective PABPN1 Ala-10/17 knockdown is the noticeable post transfection variation in the viability of HEK293T cells. Although equal amounts of DNA were transfected into cells, the viability of cells transfected with PABPN1 Ala-10 was relatively higher compared to cells transfected with PABPN Ala-17 (Figure 9). This result was expected due to previously elucidated findings indicating the role of the expanded PABPN1 Ala-17 repeat in the formation of large intranuclear protein aggregates and subsequent cell death due to the presence of insoluble INI [32, 75, 76]. Specifically, these findings supported previous studies establishing the earlier death of PABPN1 Ala-17 transfected cells compared to PABPN1 Ala-10 wildtype transfected cells [72].

The variation in cell viability between transfected cells can also be confirmed by the elevated presence of endogenous PABPN1 in the PABPN1 Ala-10/17 transfected samples. The quantification of relative endogenous PABPN1 between the samples showed an approximately 25% higher amount of endogenous PABPN1 in the presence of PABPN1-Ala 10 compared to the PABPN1 Ala-17 (Table 2 and Figure 14). This observation is consistent with the known anti-apoptotic role of endogenous wildtype PABPN1 in cell and mouse models expressing the mutant PABPN1 GCG_n repeat expansion[70].

Sample	Endogenous PABPN1				Actin				Actin / Endogenous PABPN1
	Area	Mean	Min	Max	Area	Mean	Min	Max	Normalization
PABPN1 Ala-10	637	84.21	64	103	637	106.684	91	127	1.2668804
PABPN1 Ala-17	637	59.799	39	99	637	101.215	86	120	1.6925868

Table 2. Endogenous PABPN1 western blot densitometry calculations in the presence of PABPN1 Ala-10/17

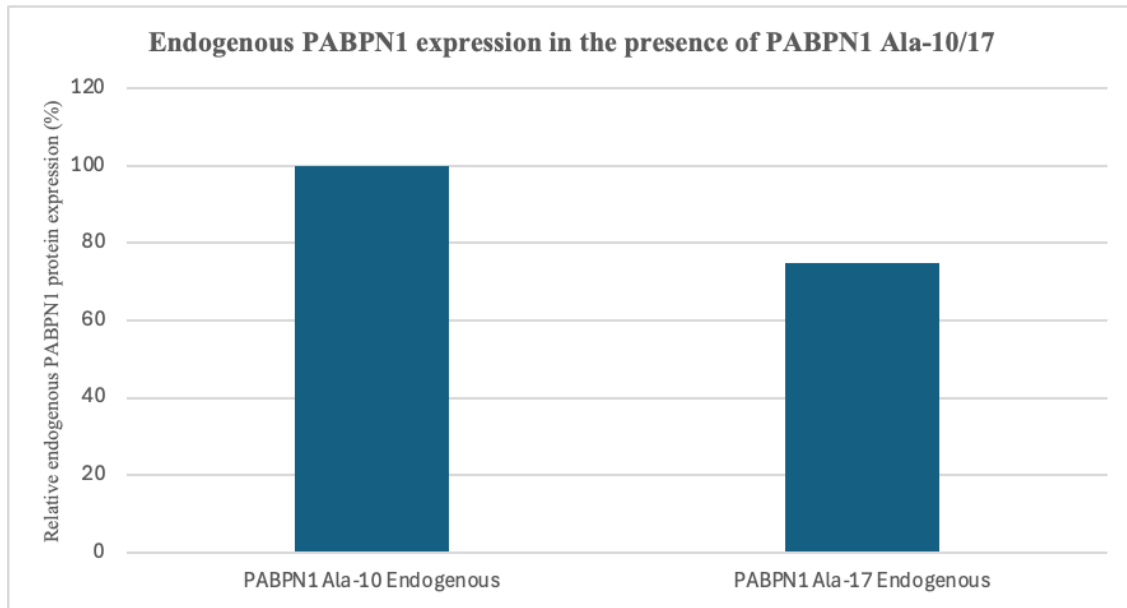


Figure 14. Relative endogenous PABPN1 expression in the presence of PABPN1 Ala-10/17

Consequently, it is apparent that diminished PABPN1 Ala-17 cell viability can confound the results of miRNA 2 knockdown by altering the observed transfection efficiency and corresponding levels of protein and RNA. When the transfection efficiency varies between PABPN1 Ala-17 and PABPN1 Ala-10, the levels of PABPN1 Ala-10/17 protein and RNA harvested can fluctuate based on transfection-induced cell death and not be purely attributed to the knockdown effect of miRNA 2. In this case, the perceived ineffectiveness or non-selectivity of miRNA 2 with respect to PABPN1 Ala-10/17 would be incorrectly attributed to its cleavage properties as opposed to variations in the starting amounts of PABPN1 Ala-10/17 protein and RNA post-transfection.

Therefore, due to the deleterious nature of PABPN1 Ala-17, a shorter transfection time may be required in order to accurately determine the comparative selective affinity of miRNA 2 because of the instability of PABPN1 protein and RNA [77, 78]. The optimal time to collect protein and RNA post transfection should be evaluated at various time points. An ideal time period cannot be too soon after transfection because a sufficient amount time would not have elapsed to observe noticeable changes in PABPN1 protein and RNA levels following a stable transfection. Conversely, an extended time period would produce the challenges stated above in the form of variations in cell viability resulting in a misattributed knockdown of protein and RNA.

5.3 Future directions

The noticeable discrepancy in these findings between protein and RNA analyses necessitates the need to repeat the experiment with biological and technical replicates. Although preliminary data showed effective PABPN1 knockdown in the presence of miRNA 2, relative selectivity for PABPN1 Ala-17 over PABPN1 Ala-10 was not observed as both alleles were

found to be indiscriminately reduced. To clearly determine the extent to which selective knockdown due to miRNA 2 is achieved, further repeated experimental testing under the same conditions must be done.

Despite the lack of selectivity for PABPN1 Ala-17, the effectiveness of miRNA 2 on PABPN1 knockdown at the protein and RNA levels encourages the evaluation of the other miRNA constructs with modifications under the same experimental conditions. As previously stated, these minor design modifications should theoretically optimize PABPN1 Ala-17 selective cleavage to provide further valuable insights into the potential use of RNAi as an effective and selectively discriminatory treatment modality. Therefore, it is premature to draw a proper, definitive conclusion on the effectiveness and selectivity for miRNA 2 with regards to PABPN1 Ala-10/17 knockdown based on preliminary data.

Another potential future direction for studies is based off previous work establishing the protective, anti-apoptotic effect of endogenous wildtype PABPN1 against INI accumulations of mutated GCG_n *PABPN1* trinucleotide repeats in cell and mouse models [70]. The expression of endogenous *PABPN1* gene in this case confers a protective effect on cells overexpressing PABPN1 ala-10/17. Consequently, as endogenous PABPN1 is known to be overexpressed in the presence of mutated PABPN1 Ala-17 (Table 2 and Figure 14) in OPMD, it may be valuable to assess the protective effect of overexpressing endogenous wildtype PABPN1 in other neurodegenerative diseases with inclusion body pathology such as polyQ diseases (HD, SCA), Parkinson's disease, amyotrophic lateral sclerosis (ALS) and Alzheimer's disease (AD) [79].

One key example has been the identification of PABPN1 as a suppressor of the accumulation of TAR DNA-binding protein 43 (TDP-43), a key ALS disease protein [80]. Specifically, PABPN1 was found to rescue cytopathological features of TDP-43 proteinopathy

by restoring normal solubility and nuclear localization of endogenous TDP-43 while also promoting an increased rate of turnover for the degradation of pathological TDP-43 [80]. The importance of the beneficial relationship between PABPN1 and TDP-43 can also be studied in other neurodegenerative disease such as ALS, frontotemporal dementia (FTD) and AD in which accumulation of TDP-43 aggregates in the central nervous system is a common feature [81].

Another interesting example of the importance of PABPN1 in neurodegenerative diseases is the presence of differentially expressed PABPN1 in AD and the relationship of PABPN1 and the mammalian suppressor of tauopathy 2 (*MSUT2*) gene [82, 83]. *MSUT2* regulates susceptibility to tau protein toxicity and it has been found to be depleted alongside PABPN1 in postmortem brain samples from a subset of AD cases with higher tau burden and increased neuronal loss [83]. Thus, this indicates a key role of PABPN1 with regards to *MSUT2* in terms of modulating tau protein pathology in AD.

Lastly, differential expression of PABPN1 has been shown to play critical roles in oncogenesis and disease progression of prostate cancer, colorectal cancer (CRC), cervical cancer (CCa), clear cell renal cell carcinoma (ccRCC), bladder cancer (BC) and non-small cell lung cancer [84-89]. In prostate cancer, CRC and CRCC PABPN1 was overexpressed and associated with poor prognosis and more aggressive tumor behavior (proliferation, invasion and metastasis) [84, 85, 87]. In these cases, PABPN1 was a key biomarker and potential therapeutic target. Conversely, overexpression of PABPN1 in CCa, BC and non-small cell lung cancer inhibited cancer progression, improved radioresistance to treatment and decreased aggressive tumor behavior [86, 88, 89]. For these cancers, elevated levels of PABPN1 enhanced cellular pathways vital to slowing cancer progression and improving resistance to ongoing treatment modalities by interacting with miRNA molecules which act as tumor suppressors or promoters [86, 88, 89].

Overall, it is abundantly clear of the extensive potential application of wildtype PABPN1 as a treatment modality within neurodegenerative diseases and numerous cancers.

Chapter 6: Conclusion

The primary aims of this study were to design miRNAs to target the mutant form of PABPN1 Ala-17, subclone the miRNA constructs for transfection into OPMD cell lines and determine the optimal miRNA constructs best suited to selectively silence mutant PABPN1 with minimal silencing of the wildtype PABPN1 allele. The first two objectives were met but the third objective remains elusive based on preliminary protein and RNA miRNA 2-induced knockdown data obtained from testing a small number of samples. The western blot and RT-qPCR data both demonstrated the effectiveness of miRNA 2 as a targeted therapy but the data was ambiguous with regards to the ability of miRNA 2 to selectively cleave and knockdown of PABPN1 Ala-17 with a higher affinity compared to PABPN1 Ala-10. The protein analysis showed a slightly higher relative reduction in PABPN1 Ala-17 over PABPN1 Ala-10 in contrast to the marginally increased reduction of PABPN1 Ala-10 expression in RT-qPCR. This experiment must be repeated with biological and technical replicates in order to definitively conclude whether the observed differences in PABPN1 protein and RNA knockdown due to miRNA 2 are concordant and biologically/statistically significant in terms of selectivity.

Despite the inconclusive evidence for selectivity, the encouraging implication of the limited data gathered from this study was that the designed miRNA construct was proven to be effective in PABPN1 Ala-10/17 knockdown. The proof of concept presented in this study based on the western blot and RT-qPCR data thus validates the approach to conduct further experimental testing with miRNA constructs to identify optimally selective sequences for RNAi. Additionally, there is optimism that the other miRNA constructs will be as effective and more selective based on variations in design. These constructs each contain certain design

modifications at particular nucleotides of the passenger and guide strands to optimize the miRNA internal loop structure for RNAi activity. In theory, incorporation of these modifications should produce a noticeable improvement in the selectivity of miRNA to cleave the intended PABPN1 Ala-17 target based on a relatively higher affinity for the GCG_n expanded repeat mutant allele. Moreover, these microRNAs were designed against GCG_n, but for optimal results that target all different mutations, more microRNAs will be designed to target the GCN_n. In conclusion, this study provides compelling evidence to suggest the potential use of RNAi as a targeted therapy in OPMD.

References

1. Kovtun, I.V. and C.T. McMurray, *Features of trinucleotide repeat instability in vivo*. Cell Res, 2008. **18**(1): p. 198-213.
2. McMahan., K., et al., *Neurogenetics in the Genome Era*. Pediatric Neurology, 2017: p. 257-267.
3. Raj, R.D., *Molecular markers and its application in animal breeding*, in *Molecular advances in Animal Genomics*. 2021. p. 123-140.
4. Brazda, V., M. Fojta, and R.P. Bowater, *Structures and stability of simple DNA repeats from bacteria*. Biochem J, 2020. **477**(2): p. 325-339.
5. van Belkum, A., et al., *Short-sequence DNA repeats in prokaryotic genomes*. Microbiol Mol Biol Rev, 1998. **62**(2): p. 275-93.
6. Yoon, J.G., et al., *Diagnostic uplift through the implementation of short tandem repeat analysis using exome sequencing*. Eur J Hum Genet, 2024. **32**(5): p. 584-587.
7. McMurray, C.T., *Mechanisms of trinucleotide repeat instability during human development*. Nat Rev Genet, 2010. **11**(11): p. 786-99.
8. Monckton, D.G. and C.T. Caskey, *Unstable triplet repeat diseases*. Circulation, 1995. **91**(2): p. 513-20.
9. Mirkin, S.M., *Expandable DNA repeats and human disease*. Nature, 2007. **447**(7147): p. 932-40.
10. Gatchel, J.R. and H.Y. Zoghbi, *Diseases of unstable repeat expansion: mechanisms and common principles*. Nat Rev Genet, 2005. **6**(10): p. 743-55.
11. Kurokawa, R., et al., *Clinical and neuroimaging review of triplet repeat diseases*. Jpn J Radiol, 2023. **41**(2): p. 115-130.
12. Verkerk, A.J., et al., *Identification of a gene (FMR-1) containing a CGG repeat coincident with a breakpoint cluster region exhibiting length variation in fragile X syndrome*. Cell, 1991. **65**(5): p. 905-14.
13. Knight, S.J., et al., *Trinucleotide repeat amplification and hypermethylation of a CpG island in FRAXE mental retardation*. Cell, 1993. **74**(1): p. 127-34.
14. Gusella, J.F., et al., *A polymorphic DNA marker genetically linked to Huntington's disease*. Nature, 1983. **306**(5940): p. 234-8.
15. *A novel gene containing a trinucleotide repeat that is expanded and unstable on Huntington's disease chromosomes. The Huntington's Disease Collaborative Research Group*. Cell, 1993. **72**(6): p. 971-83.
16. Orr, H.T., et al., *Expansion of an unstable trinucleotide CAG repeat in spinocerebellar ataxia type 1*. Nat Genet, 1993. **4**(3): p. 221-6.
17. Levinson, G. and G.A. Gutman, *Slipped-strand mispairing: a major mechanism for DNA sequence evolution*. Mol Biol Evol, 1987. **4**(3): p. 203-21.
18. Viguera, E., D. Canceill, and S.D. Ehrlich, *Replication slippage involves DNA polymerase pausing and dissociation*. EMBO J, 2001. **20**(10): p. 2587-95.
19. McMurray, C.T., *DNA secondary structure: a common and causative factor for expansion in human disease*. Proc Natl Acad Sci U S A, 1999. **96**(5): p. 1823-5.
20. Gacy, A.M., et al., *Trinucleotide repeats that expand in human disease form hairpin structures in vitro*. Cell, 1995. **81**(4): p. 533-40.

21. Shelbourne, P., et al., *Unstable DNA may be responsible for the incomplete penetrance of the myotonic dystrophy phenotype*. Hum Mol Genet, 1992. **1**(7): p. 467-73.
22. Nettleship, E., *On heredity in the various forms of cataract*. Rep. R. Lond. Ophthal. Hosp, 1905. **16**: p. 179-246.
23. Abu-Baker, A. and G.A. Rouleau, *Oculopharyngeal muscular dystrophy: recent advances in the understanding of the molecular pathogenic mechanisms and treatment strategies*. Biochim Biophys Acta, 2007. **1772**(2): p. 173-85.
24. Bouchard, J.P., et al., *Recent studies on oculopharyngeal muscular dystrophy in Quebec*. Neuromuscul Disord, 1997. **7 Suppl 1**: p. S22-9.
25. Van Der Sluijs, B.M., et al., *Oculopharyngeal muscular dystrophy with limb girdle weakness as major complaint*. J Neurol, 2003. **250**(11): p. 1307-12.
26. Little, B.W. and D.P. Perl, *Oculopharyngeal muscular dystrophy. An autopsied case from the French-Canadian kindred*. J Neurol Sci, 1982. **53**(2): p. 145-58.
27. Brais, B., et al., *Oculopharyngeal muscular dystrophy*. Semin Neurol, 1999. **19**(1): p. 59-66.
28. Brais, B., et al., *Short GCG expansions in the PABP2 gene cause oculopharyngeal muscular dystrophy*. Nat Genet, 1998. **18**(2): p. 164-7.
29. Richard, P., et al., *Correlation between PABPN1 genotype and disease severity in oculopharyngeal muscular dystrophy*. Neurology, 2017. **88**(4): p. 359-365.
30. Kroon, R., et al., *Muscle MRI in Patients With Oculopharyngeal Muscular Dystrophy: A Longitudinal Study*. Neurology, 2024. **102**(1): p. e207833.
31. Tome, F.M. and M. Fardeau, *Nuclear inclusions in oculopharyngeal dystrophy*. Acta Neuropathol, 1980. **49**(1): p. 85-7.
32. Shanmugam, V., et al., *PABP2 polyalanine tract expansion causes intranuclear inclusions in oculopharyngeal muscular dystrophy*. Ann Neurol, 2000. **48**(5): p. 798-802.
33. Nemeth, A., et al., *Isolation of genomic and cDNA clones encoding bovine poly(A) binding protein II*. Nucleic Acids Res, 1995. **23**(20): p. 4034-41.
34. Calado, A., et al., *Nuclear inclusions in oculopharyngeal muscular dystrophy consist of poly(A) binding protein 2 aggregates which sequester poly(A) RNA*. Hum Mol Genet, 2000. **9**(15): p. 2321-8.
35. Wahle, E., et al., *Mammalian poly(A)-binding protein II. Physical properties and binding to polynucleotides*. J Biol Chem, 1993. **268**(4): p. 2937-45.
36. Wahle, E., *A novel poly(A)-binding protein acts as a specificity factor in the second phase of messenger RNA polyadenylation*. Cell, 1991. **66**(4): p. 759-68.
37. Abu-Baker, A., et al., *Cytoplasmic targeting of mutant poly(A)-binding protein nuclear 1 suppresses protein aggregation and toxicity in oculopharyngeal muscular dystrophy*. Traffic, 2005. **6**(9): p. 766-79.
38. Abu-Baker, A., et al., *RNA-Based Therapy Utilizing Oculopharyngeal Muscular Dystrophy Transcript Knockdown and Replacement*. Mol Ther Nucleic Acids, 2019. **15**: p. 12-25.
39. Coiffier, L., et al., *Long-term results of cricopharyngeal myotomy in oculopharyngeal muscular dystrophy*. Otolaryngol Head Neck Surg, 2006. **135**(2): p. 218-22.
40. Kuhn, M.A. and P.C. Belafsky, *Management of cricopharyngeus muscle dysfunction*. Otolaryngol Clin North Am, 2013. **46**(6): p. 1087-99.

41. Shama, L., et al., *Surgical treatment of dysphagia*. Phys Med Rehabil Clin N Am, 2008. **19**(4): p. 817-35, ix.
42. Codere, F., *Oculopharyngeal muscular dystrophy*. Can J Ophthalmol, 1993. **28**(1): p. 1-2.
43. Rodrigue, D. and Y.M. Molgat, *Surgical correction of blepharoptosis in oculopharyngeal muscular dystrophy*. Neuromuscul Disord, 1997. **7 Suppl 1**: p. S82-4.
44. Sherman, M.Y. and A.L. Goldberg, *Cellular defenses against unfolded proteins: a cell biologist thinks about neurodegenerative diseases*. Neuron, 2001. **29**(1): p. 15-32.
45. Abu-Baker, A., et al., *Involvement of the ubiquitin-proteasome pathway and molecular chaperones in oculopharyngeal muscular dystrophy*. Hum Mol Genet, 2003. **12**(20): p. 2609-23.
46. Glover, J.R. and S. Lindquist, *Hsp104, Hsp70, and Hsp40: a novel chaperone system that rescues previously aggregated proteins*. Cell, 1998. **94**(1): p. 73-82.
47. Muchowski, P.J., et al., *Hsp70 and hsp40 chaperones can inhibit self-assembly of polyglutamine proteins into amyloid-like fibrils*. Proc Natl Acad Sci U S A, 2000. **97**(14): p. 7841-6.
48. Catoire, H., et al., *Sirtuin inhibition protects from the polyalanine muscular dystrophy protein PABPN1*. Hum Mol Genet, 2008. **17**(14): p. 2108-17.
49. Abu-Baker, A., et al., *Lithium chloride attenuates cell death in oculopharyngeal muscular dystrophy by perturbing Wnt/beta-catenin pathway*. Cell Death Dis, 2013. **4**(10): p. e821.
50. Abu-Baker, A., et al., *Valproic acid is protective in cellular and worm models of oculopharyngeal muscular dystrophy*. Neurology, 2018. **91**(6): p. e551-e561.
51. Davies, J.E., S. Sarkar, and D.C. Rubinsztein, *Trehalose reduces aggregate formation and delays pathology in a transgenic mouse model of oculopharyngeal muscular dystrophy*. Hum Mol Genet, 2006. **15**(1): p. 23-31.
52. Verheesen, P., et al., *Prevention of oculopharyngeal muscular dystrophy-associated aggregation of nuclear polyA-binding protein with a single-domain intracellular antibody*. Hum Mol Genet, 2006. **15**(1): p. 105-11.
53. Chartier, A., et al., *Prevention of oculopharyngeal muscular dystrophy by muscular expression of Llama single-chain intrabodies in vivo*. Hum Mol Genet, 2009. **18**(10): p. 1849-59.
54. Perie, S., et al., *Autologous myoblast transplantation for oculopharyngeal muscular dystrophy: a phase I/IIa clinical study*. Mol Ther, 2014. **22**(1): p. 219-25.
55. Kim, D. and J. Rossi, *RNAi mechanisms and applications*. Biotechniques, 2008. **44**(5): p. 613-6.
56. Tang, Q. and A. Khvorova, *RNAi-based drug design: considerations and future directions*. Nat Rev Drug Discov, 2024. **23**(5): p. 341-364.
57. Fire, A., et al., *Potent and specific genetic interference by double-stranded RNA in Caenorhabditis elegans*. Nature, 1998. **391**(6669): p. 806-11.
58. Lam, J.K., et al., *siRNA Versus miRNA as Therapeutics for Gene Silencing*. Mol Ther Nucleic Acids, 2015. **4**(9): p. e252.
59. Ying, S.Y., D.C. Chang, and S.L. Lin, *The microRNA (miRNA): overview of the RNA genes that modulate gene function*. Mol Biotechnol, 2008. **38**(3): p. 257-68.
60. O'Brien, J., et al., *Overview of MicroRNA Biogenesis, Mechanisms of Actions, and Circulation*. Front Endocrinol (Lausanne), 2018. **9**: p. 402.

61. Levin, A.A., *Treating Disease at the RNA Level with Oligonucleotides*. N Engl J Med, 2019. **380**(1): p. 57-70.
62. Crawford, T.O. and C.A. Pardo, *The neurobiology of childhood spinal muscular atrophy*. Neurobiol Dis, 1996. **3**(2): p. 97-110.
63. Hu, J., et al., *Allele-specific silencing of mutant huntingtin and ataxin-3 genes by targeting expanded CAG repeats in mRNAs*. Nat Biotechnol, 2009. **27**(5): p. 478-84.
64. Aronin, N., *Expanded CAG repeats in the crosshairs*. Nat Biotechnol, 2009. **27**(5): p. 451-2.
65. Malerba, A., et al., *PABPN1 gene therapy for oculopharyngeal muscular dystrophy*. Nat Commun, 2017. **8**: p. 14848.
66. Bofill-De Ros, X. and S. Gu, *Guidelines for the optimal design of miRNA-based shRNAs*. Methods, 2016. **103**: p. 157-66.
67. De, N., et al., *Highly complementary target RNAs promote release of guide RNAs from human Argonaute2*. Mol Cell, 2013. **50**(3): p. 344-55.
68. Abu-Baker, A., et al., *Current targeted therapeutic strategies for oculopharyngeal muscular dystrophy: from pharmacological to RNA replacement and gene editing therapies*. Int. J. Clin. Neurosci. Ment. Health, 2016. **3**.
69. Messaed, C., et al., *Soluble expanded PABPN1 promotes cell death in oculopharyngeal muscular dystrophy*. Neurobiol Dis, 2007. **26**(3): p. 546-57.
70. Davies, J.E., S. Sarkar, and D.C. Rubinsztein, *Wild-type PABPN1 is anti-apoptotic and reduces toxicity of the oculopharyngeal muscular dystrophy mutation*. Hum Mol Genet, 2008. **17**(8): p. 1097-108.
71. Kozera, B. and M. Rapacz, *Reference genes in real-time PCR*. J Appl Genet, 2013. **54**(4): p. 391-406.
72. Fan, X. and G.A. Rouleau, *Progress in understanding the pathogenesis of oculopharyngeal muscular dystrophy*. Can J Neurol Sci, 2003. **30**(1): p. 8-14.
73. Bass, J.J., et al., *An overview of technical considerations for Western blotting applications to physiological research*. Scand J Med Sci Sports, 2017. **27**(1): p. 4-25.
74. Aronin, N., *Target selectivity in mRNA silencing*. Gene Ther, 2006. **13**(6): p. 509-16.
75. Fan, X., et al., *Oligomerization of polyalanine expanded PABPN1 facilitates nuclear protein aggregation that is associated with cell death*. Hum Mol Genet, 2001. **10**(21): p. 2341-51.
76. Bao, Y.P., et al., *Mammalian, yeast, bacterial, and chemical chaperones reduce aggregate formation and death in a cell model of oculopharyngeal muscular dystrophy*. J Biol Chem, 2002. **277**(14): p. 12263-9.
77. Apponi, L.H., A.H. Corbett, and G.K. Pavlath, *Control of mRNA stability contributes to low levels of nuclear poly(A) binding protein 1 (PABPN1) in skeletal muscle*. Skelet Muscle, 2013. **3**(1): p. 23.
78. Phillips, B.L., et al., *Post-transcriptional regulation of Pabpn1 by the RNA binding protein HuR*. Nucleic Acids Res, 2018. **46**(15): p. 7643-7661.
79. Chung, C.G., H. Lee, and S.B. Lee, *Mechanisms of protein toxicity in neurodegenerative diseases*. Cell Mol Life Sci, 2018. **75**(17): p. 3159-3180.
80. Chou, C.C., et al., *PABPN1 suppresses TDP-43 toxicity in ALS disease models*. Hum Mol Genet, 2015. **24**(18): p. 5154-73.

81. Jo, M., et al., *The role of TDP-43 propagation in neurodegenerative diseases: integrating insights from clinical and experimental studies*. *Exp Mol Med*, 2020. **52**(10): p. 1652-1662.
82. Kavooosi, S., A. Shahraki, and R. Sheervalilou, *Identification of microRNA-mRNA Regulatory Networks with Therapeutic Values in Alzheimer's Disease by Bioinformatics Analysis*. *J Alzheimers Dis*, 2024. **98**(2): p. 671-689.
83. Wheeler, J.M., et al., *Activity of the poly(A) binding protein MSUT2 determines susceptibility to pathological tau in the mammalian brain*. *Sci Transl Med*, 2019. **11**(523).
84. Saez-Martinez, P., et al., *Dysregulation of RNA-Exosome machinery is directly linked to major cancer hallmarks in prostate cancer: Oncogenic role of PABPN1*. *Cancer Lett*, 2024. **584**: p. 216604.
85. Wang, Q.H., et al., *PABPN1 functions as a predictive biomarker in colorectal carcinoma*. *Mol Biol Rep*, 2023. **51**(1): p. 40.
86. Fang, F., et al., *Exosome-Mediated Transfer of miR-1323 from Cancer-Associated Fibroblasts Confers Radioresistance of C33A Cells by Targeting PABPN1 and Activating Wnt/beta-Catenin Signaling Pathway in Cervical Cancer*. *Reprod Sci*, 2022. **29**(6): p. 1809-1821.
87. Xiong, M., et al., *PABPN1 promotes clear cell renal cell carcinoma progression by suppressing the alternative polyadenylation of SGPL1 and CREG1*. *Carcinogenesis*, 2023. **44**(7): p. 576-586.
88. Chen, L., et al., *PABPN1 regulates mRNA alternative polyadenylation to inhibit bladder cancer progression*. *Cell Biosci*, 2023. **13**(1): p. 45.
89. Ichinose, J., et al., *Alternative polyadenylation is associated with lower expression of PABPN1 and poor prognosis in non-small cell lung cancer*. *Cancer Sci*, 2014. **105**(9): p. 1135-41.